Eur. Phys. J. C 23, 597–613 (2002)
Digital Object Identifier (DOI) 10.1007/s100520200926

THE EUROPEAN PHYSICAL JOURNAL C

Particle multiplicity of unbiased gluon jets from e^+e^- three-jet events

The OPAL Collaboration

G. Abbiendi[2], C. Ainsley[5], P.F. Åkesson[3], G. Alexander[22], J. Allison[16], G. Anagnostou[1], K.J. Anderson[9], S. Arcelli[17], S. Asai[23], D. Axen[27], G. Azuelos[18,a], I. Bailey[26], E. Barberio[8], R.J. Barlow[16], R.J. Batley[5], P. Bechtle[25], T. Behnke[25], K.W. Bell[20], P.J. Bell[1], G. Bella[22], A. Bellerive[6], G. Benelli[4], S. Bethke[32], O. Biebel[32], I.J. Bloodworth[1], O. Boeriu[10], P. Bock[11], J. Böhme[25], D. Bonacorsi[2], M. Boutemeur[31], S. Braibant[8], L. Brigliadori[2], R.M. Brown[20], H.J. Burckhart[8], J. Cammin[3], S. Campana[4], R.K. Carnegie[6], B. Caron[28], A.A. Carter[13], J.R. Carter[5], C.Y. Chang[17], D.G. Charlton[1,b], P.E.L. Clarke[15], E. Clay[15], I. Cohen[22], J. Couchman[15], A. Csilling[8,i], M. Cuffiani[2], S. Dado[21], G.M. Dallavalle[2], S. Dallison[16], A. De Roeck[8], E.A. De Wolf[8], P. Dervan[15], K. Desch[25], B. Dienes[30], M. Donkers[6], J. Dubbert[31], E. Duchovni[24], G. Duckeck[31], I.P. Duerdoth[16], E. Etzion[22], F. Fabbri[2], L. Feld[10], P. Ferrari[12], F. Fiedler[8], I. Fleck[10], M. Ford[5], A. Frey[8], A. Fürtjes[8], D.I. Futyan[16], P. Gagnon[12], J.W. Gary[4], G. Gaycken[25], C. Geich-Gimbel[3], G. Giacomelli[2], P. Giacomelli[2], M. Giunta[4], J. Goldberg[21], K. Graham[26], E. Gross[24], J. Grunhaus[22], M. Gruwé[8], P.O. Günther[3], A. Gupta[9], C. Hajdu[29], M. Hamann[25], G.G. Hanson[12], K. Harder[25], A. Harel[21], M. Harin-Dirac[4], M. Hauschild[8], J. Hauschildt[25], C.M. Hawkes[1], R. Hawkings[8], R.J. Hemingway[6], C. Hensel[25], G. Herten[10], R.D. Heuer[25], J.C. Hill[5], K. Hoffman[9], R.J. Homer[1], D. Horváth[29,c], K.R. Hossain[28], R. Howard[27], P. Hüntemeyer[25], P. Igo-Kemenes[11], K. Ishii[23], A. Jawahery[17], H. Jeremie[18], C.R. Jones[5], P. Jovanovic[1], T.R. Junk[6], N. Kanaya[26], J. Kanzaki[23], G. Karapetian[18], D. Karlen[6], V. Kartvelishvili[16], K. Kawagoe[23], T. Kawamoto[23], R.K. Keeler[26], R.G. Kellogg[17], B.W. Kennedy[20], D.H. Kim[19], K. Klein[11], A. Klier[24], S. Kluth[32], T. Kobayashi[23], M. Kobel[3], T.P. Kokott[3], S. Komamiya[23], R.V. Kowalewski[26], T. Krämer[25], T. Kress[4], P. Krieger[6,p], J. von Krogh[11], D. Krop[12], T. Kuhl[25], M. Kupper[24], P. Kyberd[13], G.D. Lafferty[16], H. Landsman[21], D. Lanske[14], I. Lawson[26], J.G. Layter[4], A. Leins[31], D. Lellouch[24], J. Letts[12], L. Levinson[24], J. Lillich[10], C. Littlewood[5], S.L. Lloyd[13], F.K. Loebinger[16], J. Lu[27], J. Ludwig[10], A. Macchiolo[18], A. Macpherson[28,l], W. Mader[3], S. Marcellini[2], T.E. Marchant[16], A.J. Martin[13], J.P. Martin[18], G. Martinez[17], G. Masetti[2], T. Mashimo[23], P. Mättig[24], W.J. McDonald[28], J. McKenna[27], T.J. McMahon[1], R.A. McPherson[26], F. Meijers[8], P. Mendez-Lorenzo[31], W. Menges[25], F.S. Merritt[9], H. Mes[6,a], A. Michelini[2], S. Mihara[23], G. Mikenberg[24], D.J. Miller[15], S. Moed[21], W. Mohr[10], T. Mori[23], A. Mutter[10], K. Nagai[13], I. Nakamura[23], H.A. Neal[33], R. Nisius[8], S.W. O'Neale[1], A. Oh[8], A. Okpara[11], M.J. Oreglia[9], S. Orito[23], C. Pahl[32], G. Pásztor[8,i], J.R. Pater[16], G.N. Patrick[20], J.E. Pilcher[9], J. Pinfold[28], D.E. Plane[8], B. Poli[2], J. Polok[8], O. Pooth[8], A. Quadt[3], K. Rabbertz[8], C. Rembser[8], P. Renkel[24], H. Rick[4], N. Rodning[28], J.M. Roney[26], S. Rosati[3], K. Roscoe[16], Y. Rozen[21], K. Runge[10], D.R. Rust[12], K. Sachs[6], T. Saeki[23], O. Sahr[31], E.K.G. Sarkisyan[8,m,n], A.D. Schaile[31], O. Schaile[31], P. Scharff-Hansen[8], M. Schröder[8], M. Schumacher[25], C. Schwick[8], W.G. Scott[20], R. Seuster[14,g], T.G. Shears[8,j], B.C. Shen[4], C.H. Shepherd-Themistocleous[5], P. Sherwood[15], A. Skuja[17], A.M. Smith[8], G.A. Snow[17], R. Sobie[26], S. Söldner-Rembold[31,e], S. Spagnolo[20], F. Spano[9], M. Sproston[20], A. Stahl[3], K. Stephens[16], D. Strom[19], R. Ströhmer[31], L. Stumpf[26], B. Surrow[25], S. Tarem[21], M. Tasevsky[8], R.J. Taylor[15], R. Teuscher[9], J. Thomas[15], M.A. Thomson[5], E. Torrence[19], D. Toya[23], T. Trefzger[31], A. Tricoli[2], I. Trigger[8], Z. Trócsányi[30,f], E. Tsur[22], M.F. Turner-Watson[1], I. Ueda[23], B. Ujvári[30,f], B. Vachon[26], C.F. Vollmer[31], P. Vannerem[10], M. Verzocchi[17], H. Voss[8], J. Vossebeld[8], D. Waller[6], C.P. Ward[5], D.R. Ward[5], P.M. Watkins[1], A.T. Watson[1], N.K. Watson[1], P.S. Wells[8], T. Wengler[8], N. Wermes[3], D. Wetterling[11] G.W. Wilson[16,o], J.A. Wilson[1], T.R. Wyatt[16], S. Yamashita[23], V. Zacek[18], D. Zer-Zion[8,k]

[1] School of Physics and Astronomy, University of Birmingham, Birmingham B15 2TT, UK
[2] Dipartimento di Fisica dell' Università di Bologna and INFN, 40126 Bologna, Italy
[3] Physikalisches Institut, Universität Bonn, 53115 Bonn, Germany
[4] Department of Physics, University of California, Riverside CA 92521, USA
[5] Cavendish Laboratory, Cambridge CB3 0HE, UK
[6] Ottawa-Carleton Institute for Physics, Department of Physics, Carleton University, Ottawa, Ontario K1S 5B6, Canada
[8] CERN, European Organization for Nuclear Research, 1211 Geneva 23, Switzerland
[9] Enrico Fermi Institute and Department of Physics, University of Chicago, Chicago IL 60637, USA
[10] Fakultät für Physik, Albert Ludwigs Universität, 79104 Freiburg, Germany
[11] Physikalisches Institut, Universität Heidelberg, 69120 Heidelberg, Germany
[12] Indiana University, Department of Physics, Swain Hall West 117, Bloomington IN 47405, USA

[13] Queen Mary and Westfield College, University of London, London E1 4NS, UK
[14] Technische Hochschule Aachen, III Physikalisches Institut, Sommerfeldstrasse 26-28, 52056 Aachen, Germany
[15] University College London, London WC1E 6BT, UK
[16] Department of Physics, Schuster Laboratory, The University, Manchester M13 9PL, UK
[17] Department of Physics, University of Maryland, College Park, MD 20742, USA
[18] Laboratoire de Physique Nucléaire, Université de Montréal, Montréal, Quebec H3C 3J7, Canada
[19] University of Oregon, Department of Physics, Eugene OR 97403, USA
[20] CLRC Rutherford Appleton Laboratory, Chilton, Didcot, Oxfordshire OX11 0QX, UK
[21] Department of Physics, Technion-Israel Institute of Technology, Haifa 32000, Israel
[22] Department of Physics and Astronomy, Tel Aviv University, Tel Aviv 69978, Israel
[23] International Centre for Elementary Particle Physics and Department of Physics, University of Tokyo, Tokyo 113-0033, and Kobe University, Kobe 657-8501, Japan
[24] Particle Physics Department, Weizmann Institute of Science, Rehovot 76100, Israel
[25] Universität Hamburg/DESY, II Institut für Experimental Physik, Notkestrasse 85, 22607 Hamburg, Germany
[26] University of Victoria, Department of Physics, P O Box 3055, Victoria BC V8W 3P6, Canada
[27] University of British Columbia, Department of Physics, Vancouver BC V6T 1Z1, Canada
[28] University of Alberta, Department of Physics, Edmonton AB T6G 2J1, Canada
[29] Research Institute for Particle and Nuclear Physics, 1525 Budapest, P O Box 49, Hungary
[30] Institute of Nuclear Research, 4001 Debrecen, P O Box 51, Hungary
[31] Ludwigs-Maximilians-Universität München, Sektion Physik, Am Coulombwall 1, 85748 Garching, Germany
[32] Max-Planck-Institute für Physik, Föhring Ring 6, 80805 München, Germany
[33] Yale University, Department of Physics, New Haven, CT 06520, USA

Received: 25 October 2001 / Revised version: 20 January 2002 /
Published online: 5 April 2002 –

Abstract. The charged particle multiplicities of two- and three-jet events from the reaction $e^+e^- \to Z^0 \to$ *hadrons* are measured for Z^0 decays to light quark (uds) flavors. Using recent theoretical expressions to account for biases from event selection, results corresponding to unbiased gluon jets are extracted over a range of jet energies from about 11 to 30 GeV. We find consistency between these results and direct measurements of unbiased gluon jet multiplicity from Υ and Z^0 decays. The unbiased gluon jet data including the direct measurements are compared to corresponding results for quark jets. We perform fits based on analytic expressions for particle multiplicity in jets to determine the ratio $r \equiv N_g/N_q$ of multiplicities between gluon and quark jets as a function of energy. We also determine the ratio of slopes, $r^{(1)} \equiv (dN_g/dy)/(dN_q/dy)$, and of curvatures, $r^{(2)} \equiv (d^2N_g/dy^2)/(d^2N_q/dy^2)$, where y specifies the energy scale. At 30 GeV, we find $r = 1.422 \pm 0.051$, $r^{(1)} = 1.761 \pm 0.071$ and $r^{(2)} = 1.98 \pm 0.13$, where the uncertainties are the statistical and systematic terms added in quadrature. These results are in general agreement with theoretical predictions. In addition, we use the measurements of the energy dependence of N_g and N_q to determine an effective value of the ratio of QCD color factors, C_A/C_F. Our result, $C_A/C_F = 2.23 \pm 0.14\,(\text{total})$, is consistent with the QCD value of 2.25.

1 Introduction

The mean charged particle multiplicity of a gluon jet has often been measured in the annihilation of an electron and positron to hadrons, $e^+e^- \to$ *hadrons*. The usual method (see for example [1]–[4]) is to select three-jet quark-antiquark-gluon $q\bar{q}g$ final states for which the events and individual jets are defined using a jet algorithm such as the Durham [5] or Luclus [6] jet finder. The particle multiplicity of a jet determined with this technique is found to depend on which algorithm is employed. Therefore, these jets and the associated $q\bar{q}g$ events are called "biased."

In contrast, theoretical calculations usually define gluon jet multiplicity inclusively, by the particles in hemispheres of gluon-gluon (gg) systems in an overall color singlet. Quark jets are defined analogously as hemispheres of quark-antiquark ($q\bar{q}$) systems. The hemisphere defini-

[a] and at TRIUMF, Vancouver, Canada V6T 2A3
[b] and Royal Society University Research Fellow
[c] and Institute of Nuclear Research, Debrecen, Hungary
[e] and Heisenberg Fellow
[f] and Department of Experimental Physics, Lajos Kossuth University, Debrecen, Hungary
[g] and MPI München
[i] and Research Institute for Particle and Nuclear Physics, Budapest, Hungary
[j] now at University of Liverpool, Dept of Physics, Liverpool L69 3BX, UK
[k] and University of California, Riverside, High Energy Physics Group, CA 92521, USA
[l] and CERN, EP Div, 1211 Geneva 23
[m] and Universitaire Instelling Antwerpen, Physics Department, B-2610 Antwerpen, Belgium
[n] and Tel Aviv University, School of Physics and Astronomy, Tel Aviv 69978, Israel
[o] now at University of Kansas, Dept of Physics and Astronomy, Lawrence, KS 66045, USA
[p] now at University of Toronto, Dept of Physics, Toronto, Canada

tion of jets yields results which are independent of a jet finder. Therefore, these jets are called "unbiased." Unbiased gluon jet multiplicity has so far been measured only in Υ [7,8] and Z^0 [9]- [11] decays, corresponding to jet energies of about 5 and 40 GeV, respectively. In contrast, unbiased quark jet multiplicity is easy to measure and has been determined at many scales (for a recent review, see [12]).

It is of interest to measure unbiased gluon jet multiplicity at other scales. Such measurements would allow a test of recent predictions [13,14] from Quantum Chromodynamics (QCD) for the scale dependence of the multiplicity ratio r between gluon and quark jets and for the related ratios of slopes $r^{(1)}$ and of curvatures $r^{(2)}$:

$$r \equiv \frac{\mathrm{N}_g}{\mathrm{N}_q} \quad , \tag{1}$$

$$r^{(1)} \equiv \frac{\mathrm{d}\mathrm{N}_g/\mathrm{d}y}{\mathrm{d}\mathrm{N}_q/\mathrm{d}y} \quad , \tag{2}$$

$$r^{(2)} \equiv \frac{\mathrm{d}^2\mathrm{N}_g/\mathrm{d}^2y}{\mathrm{d}^2\mathrm{N}_q/\mathrm{d}^2y} \quad , \tag{3}$$

where N_g and N_q are the mean particle multiplicities of gluon and quark jets, $y = \ln(Q/\Lambda)$, Q is the jet energy and Λ is the QCD scale parameter. Recently, a method to extract unbiased gluon jet multiplicity from *biased* $e^+e^- \to q\overline{q}g$ events was proposed [15,16], extending earlier formalism [17]. This method provides an indirect means to determine the particle multiplicity of gluon jets, in a manner which corresponds to the hemisphere definition of jets. By combining measurements of N_g found from this method with the unbiased measurements for N_q, the ratios r, $r^{(1)}$ and $r^{(2)}$ can be determined at a variety of scales and used to test the corresponding QCD results in a quantitative manner.

The purpose of the present study is to test this method [15,16] to obtain unbiased measurements of N_g and to apply the results to determine the ratios, (1)–(3). The data were collected with the OPAL detector operating at the LEP accelerator at CERN. We determine the ratios (1)–(3) as a function of scale and compare the results to recent QCD predictions [13,14]. Previously published measurements of the scale dependence of r [4,18,19] and $r^{(1)}$ [18, 19] were based on biased jet samples, whereas experimental results for the ratio of curvatures $r^{(2)}$ have not previously been presented. We also use the results on the scale dependence of unbiased gluon and quark jet multiplicities to derive a measurement of the ratio of QCD color factors $C_\mathrm{A}/C_\mathrm{F}$.

2 Theoretical framework

Analytic expressions for the mean particle multiplicity of e^+e^- three-jet events, valid in the modified leading logarithmic approximation of perturbation theory (MLLA [20]), were recently presented in [16]:

$$\mathrm{N}_{q\overline{q}g} = \mathrm{N}_{q\overline{q}}\left(L, k_{\perp,Lu}\right) + \frac{1}{2}\,\mathrm{N}_{gg}\left(k_{\perp,Lu}\right) \quad , \tag{4}$$

$$\mathrm{N}_{q\overline{q}g} = \mathrm{N}_{q\overline{q}}\left(L_{q\overline{q}}, k_{\perp,Lu}\right) + \frac{1}{2}\,\mathrm{N}_{gg}\left(k_{\perp,Le}\right) \quad . \tag{5}$$

These results, along with the others presented in this section, are based on massless quarks. The reason for the two different expressions, (4) and (5), is that there is an ambiguity in the definition of the gluon jet transverse momentum when the gluon radiation is hard. $k_{\perp,Lu}$ and $k_{\perp,Le}$ are the transverse momenta of the gluon with respect to the quark-antiquark system using the definition of either the Lund ($k_{\perp,Lu}$) [15] or Leningrad ($k_{\perp,Le}$) [17] groups, see [16] and references therein for further discussion. Note that due to QCD coherence, the multiplicity of a gluon jet produced in e^+e^- annihilations depends on its transverse momentum and not its energy (see for example [17]). $\mathrm{N}_{q\overline{q}g}$ is the particle multiplicity of a three-jet event selected using a jet algorithm (see below). $\mathrm{N}_{q\overline{q}}$ and N_{gg} are the multiplicities of two-jet $q\overline{q}$ and gg systems, given by twice N_q and N_g, respectively. The scales L, $L_{q\overline{q}}$, $k_{\perp,Lu}$ and $k_{\perp,Le}$ are defined as follows:

$$L = \ln\left(\frac{s}{\Lambda^2}\right) \quad , \tag{6}$$

$$L_{q\overline{q}} = \ln\left(\frac{s_{q\overline{q}}}{\Lambda^2}\right) \quad , \tag{7}$$

$$k_{\perp,Lu} = 2\,\ln\left(\frac{p_{\perp,Lu}}{\Lambda}\right) \quad , \tag{8}$$

$$k_{\perp,Le} = 2\,\ln\left(\frac{p_{\perp,Le}}{\Lambda}\right) \quad , \tag{9}$$

$$s_{q\overline{q}} = p_q \cdot p_{\overline{q}} \quad , \tag{10}$$

$$p_{\perp,Lu} = \sqrt{\frac{s_{qg}s_{\overline{q}g}}{s}} \quad , \tag{11}$$

$$p_{\perp,Le} = \sqrt{\frac{s_{qg}s_{\overline{q}g}}{s_{q\overline{q}}}} \quad , \tag{12}$$

with $s = E^2_{c.m.}$, $s_{ig} = p_i \cdot p_g$ $(i = q, \overline{q})$, and p_q, $p_{\overline{q}}$ and p_g the 4-momenta of the q, $\overline{q}$ and g. L specifies the e^+e^- c.m. energy ($E_{c.m.}$) and $L_{q\overline{q}}$ the energy of the $q\overline{q}$ system in the $q\overline{q}$ rest frame.

The multiplicity of the gg system in this formalism, N_{gg}, depends only on a single scale: $k_{\perp,Lu}$ in (4) or $k_{\perp,Le}$ in (5). This dependence on a single scale is a statement that N_{gg} is *unbiased*, i.e. $\mathrm{N}_{gg}(k_\perp)$ in (4) or (5) is equivalent to the inclusive multiplicity of a gg event from a color singlet source produced at the same scale $k_\perp$, to MLLA accuracy. In contrast, the multiplicity of the $q\overline{q}$ system, $\mathrm{N}_{q\overline{q}}$, depends on *two* scales: L and $k_{\perp,Lu}$ in (4) or $L_{q\overline{q}}$ and $k_{\perp,Lu}$ in (5). This dependence on two scales implies that the multiplicity of the $q\overline{q}$ system is *biased*, depending on a hard scale L or $L_{q\overline{q}}$ for the production of the quark and antiquark jets and on a cutoff $k_\perp \approx k_{\perp,Lu}$ below which the gluon jet is not resolved. This accounting for the bias in quark jet multiplicity due to the jet finder criteria used to select the $q\overline{q}g$ events is the difference between the theoretical results used here [15] and those presented previously [17].

The above expressions are valid for jet algorithms which employ a transverse momentum cutoff $k_\perp$ to resolve "two-jet" $q\overline{q}$ from "three-jet" $q\overline{q}g$ events. Examples of such algorithms are the Durham [5], Cambridge [21]

and Luclus [6] jet finders. The formalism is not expected to be valid for the Jade [22] or cone jet finders [23], which use invariant masses or angles rather than transverse momenta to separate the two- and three-jet event classes.

According to the prescription in [16], the resolution scale $k_\perp$ should be adjusted separately for each event so exactly three jets are reconstructed. In contrast, a fixed value of the resolution scale results in truncation of higher order radiation, biasing the gluon jet's properties. Note that any radiation ("sub-jet") emitted within the quark or gluon jet must necessarily have a smaller transverse momentum than the gluon jet itself: otherwise the role of the "gluon jet" and "sub-jet" would be reversed. Thus the transverse momentum of the gluon jet, $k_{\perp,gluon}$, defines an effective cutoff for sub-jet radiation, i.e. $k_\perp = k_{\perp,gluon} \approx k_{\perp,Lu}$.

In the formalism of [15], the biased quark jet multiplicities $\mathrm{N}_{q\bar{q}}(J, k_{\perp,Lu})$ in (4) and (5) (with J representing either L or $L_{q\bar{q}}$) can be obtained from the corresponding *unbiased* multiplicities $\mathrm{N}_{q\bar{q}}(J')$, which depend only on a single scale J', through the relation:

$$\mathrm{N}_{q\bar{q}}(J, k_{\perp,Lu}) \;=\; \mathrm{N}_{q\bar{q}}(J') + (J - J')\,\frac{\mathrm{d}\,\mathrm{N}_{q\bar{q}}(J')}{\mathrm{d}J'} \quad , \quad (13)$$

where $J' = k_{\perp,Lu} + c_q$ with $c_q = 3/2$. The unbiased term $\mathrm{N}_{q\bar{q}}(K)$ is equivalent to the mean multiplicity of inclusive $e^+e^- \to hadrons$ events as a function of $K = E_{c.m.}$.

Finally, a relationship between the scale evolution of unbiased gluon and quark jet multiplicities is given [15]:

$$\frac{\mathrm{d}\,\mathrm{N}_{gg}(L')}{\mathrm{d}L} = \frac{C_\mathrm{A}}{C_\mathrm{F}}\left(1 - \frac{\alpha_0 c_r}{L}\right)\frac{\mathrm{d}\,\mathrm{N}_{q\bar{q}}(L)}{\mathrm{d}L} \quad , \quad (14)$$

where $L' = L + c_g - c_q$, $c_g = 11/6$, $\alpha_0 = 6\,C_\mathrm{A}/(11\,C_\mathrm{A} - 2\,n_f)$, $c_r = 10\,\pi^2/27 - 3/2$, and n_f equals the number of active quark flavors, taken to be $n_f = 5$. C_A and C_F are the QCD color factors, 3 and 4/3, respectively.

3 Detector and data sample

The OPAL detector is described in detail elsewhere [24, 25]. The tracking system consists of a silicon microvertex detector, an inner vertex chamber, a large volume jet chamber, and specialized chambers at the outer radius of the jet chamber which improve the measurements in the z-direction[1]. The tracking system covers the region $|\cos\theta| < 0.98$ and is enclosed by a solenoidal magnet coil with an axial field of 0.435 T. Electromagnetic energy is measured by a lead-glass calorimeter located outside the magnet coil, which also covers $|\cos\theta| < 0.98$.

The present analysis is based on a sample of about 2 283 000 hadronic annihilation events, corresponding to the OPAL sample collected within 0.3 GeV of the Z^0 peak that includes readout of both the r-ϕ and z coordinates of the silicon strip microvertex detector [25]. The procedures for identifying hadronic annihilation events are described in [26].

We employ charged tracks measured in the tracking chambers and clusters measured in the electromagnetic calorimeter. Charged tracks are required to have at least 20 measured points (of 159 possible) in the jet chamber, or at least 50% of the points expected based on the track's polar angle, whichever is smaller. In addition, the tracks are required to have a momentum in the direction perpendicular to the beam axis greater than 0.05 GeV/c, to lie in the region $|\cos\theta| < 0.96$, to point to the origin to within 5 cm in the r-ϕ plane and 30 cm in the z direction, and to yield a reasonable χ^2 per degree-of-freedom (d.o.f.) for the track fit in the r-ϕ plane. Clusters are required to have an energy greater than 0.10 GeV if they are in the barrel section of the detector ($|\cos\theta| < 0.82$) or 0.25 GeV if they are in the endcap section ($0.82 < |\cos\theta| < 0.98$). A matching algorithm is employed to reduce double counting of energy in cases where charged tracks point towards electromagnetic clusters. Specifically, the expected calorimeter energy of the associated tracks is subtracted from the cluster energy. If the energy of a cluster is smaller than that expected for the associated tracks, the cluster is not used. Each accepted track and cluster is considered to be a particle. Tracks are assigned the pion mass. Clusters are assigned zero mass since they originate mostly from photons.

To eliminate residual background and events in which a significant number of particles is lost near the beam direction, the number of accepted charged tracks in an event is required to be at least five and the thrust axis [27] of the event, calculated using the particles, is required to satisfy $|\cos(\theta_\mathrm{thrust})| < 0.90$, where θ_thrust is the angle between the thrust and beam axes. The residual background to the sample of hadronic events from all sources is estimated to be less than 1% [26].

4 Selection of uds events

The theoretical formalism we employ is based on massless quarks, as stated in Sect. 2. Therefore, beginning with the data sample described in Sect. 3, we select light quark (u, d and s) events for our study.

The uds event tagging is based on the signed impact parameter values of charged tracks with respect to the primary event vertex, d_{sign}. The magnitude of d_{sign} is given by the distance of closest approach of the track to the event vertex in the r-ϕ plane. The sign of d_{sign} is determined as follows. Jets are reconstructed in each event using the cone jet finder [23][2]. For each track assigned to a jet by the jet finder, hemispheres are defined by the plane perpendicular to the corresponding jet axis. The sign of d_{sign} is determined using the crossing point in the r-ϕ plane between the track and jet axis to which it is assigned. d_{sign} is positive if the crossing point is in the

[1] Our coordinate system is defined so that z is the coordinate parallel to the e^- beam axis, r is the coordinate normal to the beam axis, ϕ is the azimuthal angle around the beam axis and θ is the polar angle with respect to z

[2] The jet resolution parameters used are: a cone half angle of 0.55 radians and a minimum jet energy of 5 GeV

forward hemisphere and negative otherwise. The forward hemisphere is the hemisphere which contains the jet. Because of the relatively long lifetime of hadrons containing c and b quarks, the distribution of d_{sign} is strongly skewed toward positive values for c and b events but not for uds events.

Note that the jet finding procedure described in the previous paragraph is employed solely for the purpose of identifying uds events and not for the analysis of gluon jet multiplicity presented below in Sects. 5-6.

Charged tracks are selected for the uds tagging procedure if they have r-ϕ coordinate information from at least one of the two silicon detector layers, a momentum of 1 GeV/c or larger, and a maximum distance of closest approach to the primary event vertex in the r-ϕ plane of 0.3 cm with a maximum uncertainty on this quantity of 0.1 cm. In addition they must be assigned to a jet using the cone jet finding procedure mentioned above. If no track in an event satisfies these requirements (1.5% of the events), the event is eliminated[3]. The number of tracks which meet these requirements and have $d_{sign}/\sigma_{d_{sign}} > 3.0$ is determined, where $\sigma_{d_{sign}}$ is the uncertainty associated with d_{sign}. An event is tagged as a uds event if this number is zero. In total 1 109 017 events are tagged. The number of events in our final event sample and the corresponding uds purity are presented in Sect. 5.

5 Analysis method

Three-jet events are defined using a jet algorithm. For our standard analysis we employ the Durham jet finder [5]. As a systematic check, we use the Cambridge [21] and Luclus [6] jet finders (see Sect. 7). We choose these algorithms because they employ a cutoff in transverse momentum to separate two- and three-jet events, in correspondence to the theoretical formalism of [15,16]. In particular, this means that (4), (5), (13) and (14) are expected to be applicable for these jet algorithms.

The resolution scale of the Durham jet finder, y_{cut}, is adjusted separately for each tagged uds event so exactly three jets are reconstructed. For the Cambridge jet finder, the resolution scale is again y_{cut}. For Luclus, the corresponding parameter is d_{join}. We apply this procedure rather than use a fixed resolution scale to avoid introducing a bias in the gluon jet properties as discussed in Sect. 2. The jets are assigned energies based on the angles between them, assuming massless kinematics (see for example [28]). The jets are ordered from 1 to 3 such that jet 1 has the highest energy. Events are retained if the angles between the highest energy jet and the other two are the same to within 3°, the so-called "Y events"[4]. A schematic diagram of a Y event is shown in Fig. 1. For Y events, the scales $L_{q\bar{q}}$, $k_{\perp,Lu}$ and $k_{\perp,Le}$ (7)–(9) depend only on $E_{c.m.}$ and one inter-jet angle, conveniently chosen to be θ_1 (see Fig. 1). For $35° \le \theta_1 \le 120°$, the range of θ_1 we employ for our gluon jet analysis (Sect. 6.2), 22 365 events are selected: this is our final event sample. We require $\theta_1 \ge 35°$ in order that the two lower energy jets be clearly separated from each other. Note that since θ_2 and θ_3 (see Fig. 1) are not exactly equal, the energies of jets 2 and 3 are not exactly the same.

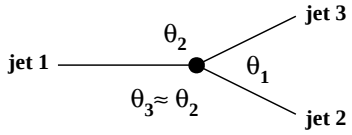

Fig. 1. Schematic representation of a three-jet quark-antiquark-gluon $q\bar{q}g$ event with a Y event topology [28,29], in which the angle between the highest energy jet and each of the two lower energy jets is about the same. The jets are ordered in energy such that jet 1 has the highest energy. The angle θ_1 opposite the highest energy jet is used to specify the event topology. In our analysis, the gluon jet is assumed to be jet 3

The uds event purity of this sample is estimated using the Jetset Monte Carlo multihadronic event generator [30] including initial state photon radiation, detector simulation [31], and the same analysis procedures as are applied to the data. We use a sample of about 6 000 000 Monte Carlo events generated with version 7.4 of the program and the parameters given in [32]. The estimated uds purity is found to be $(78.5 \pm 0.2\,(\text{stat.}))\%$. The Monte Carlo predicts that 70% of the background events are c events and 30% are b events. The ratio of the number of events in the final sample to the number in the initial multihadronic Z^0 decay sample is $(0.980 \pm 0.007\,(\text{stat.})) \times 10^{-2}$ for the data and $(1.036 \pm 0.004\,(\text{stat.})) \times 10^{-2}$ for the Monte Carlo[5].

For simplicity, we identify the gluon jet by assuming it is the lowest energy jet in an event, i.e. jet 3. For the majority of Y events, $\theta_1 << \theta_2, \theta_3$. For these events, jet 1 has an overwhelming probability (typically about 97%) to be a quark (or antiquark) jet, while jets 2 and 3 have about an equal probability to arise from a quark or gluon. Since $\theta_2 \approx \theta_3$ (see Fig. 1), the scales $L_{q\bar{q}}$, $k_{\perp,Lu}$ and $k_{\perp,Le}$ are almost unchanged if the gluon is actually jet 2 rather than jet 3. Similarly, as the energy of jet 3 increases so that $\theta_1 \approx \theta_2 \approx \theta_3$, all three jets have about the same probability to be the gluon jet and the determination of scales is again insensitive to whether the gluon jet assignment is correct or not. This relative insensitivity to gluon jet misidentification is our motivation for employing Y events.

The scales $L_{q\bar{q}}$, $k_{\perp,Lu}$ and $k_{\perp,Le}$ and the three-jet event charged particle multiplicity $N^{ch.}_{q\bar{q}g}$ are measured as a func-

[3] The vast majority of events which are so eliminated are low multiplicity events which appear in the forward region of the detector corresponding to $|\cos(\theta_{\text{thrust}})| > 0.80$, outside the acceptance of the silicon microvertex detector: the tracks in the eliminated events do not satisfy the requirement that they include at least one hit from the microvertex detector

[4] Y events were first studied in [28,29]; the overall charged multiplicity of Y events was first presented in [18]

[5] The 5% discrepancy between the selected event rates in the data and Monte Carlo is due to a small deficiency in the Monte Carlo description of the distribution of angles between the jets. The properties of the selected Y events are well described by the simulation, however, see Fig. 2. Thus this discrepancy has a negligible impact on the results of our analysis

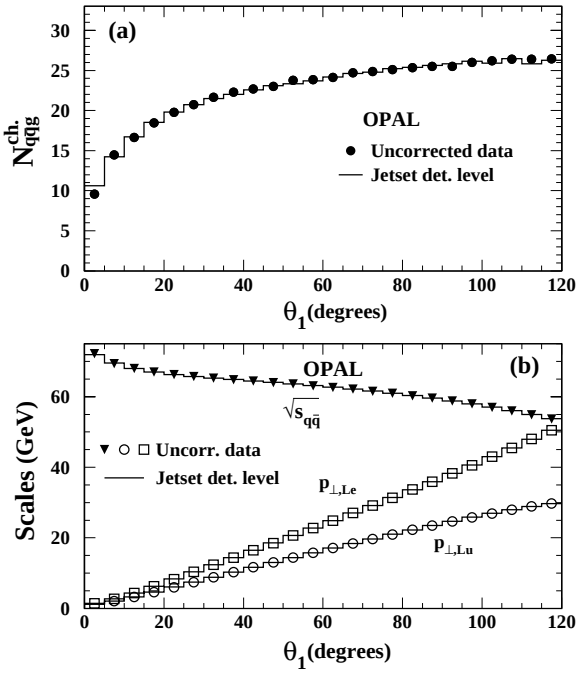

Fig. 2. a The uncorrected distribution of the mean charged particle multiplicity of three-jet uds tagged Y events from Z^0 decays as a function of the opening angle θ_1. The events are selected using the Durham [5] jet finder. **b** The corresponding distributions of the scales $\sqrt{s_{q\bar{q}}}$, $p_{\perp,Lu}$ and $p_{\perp,Le}$, see (10)–(12). The data are compared to the predictions of the Jetset Monte Carlo. The Jetset predictions are presented at the detector level, i.e. including initial-state radiation, detector simulation, and the same analysis procedures as are applied to the data. Therefore both the data and Monte Carlo results include the background from non-uds events and gluon jet misidentification. The uncertainties (too small to be visible) are statistical only

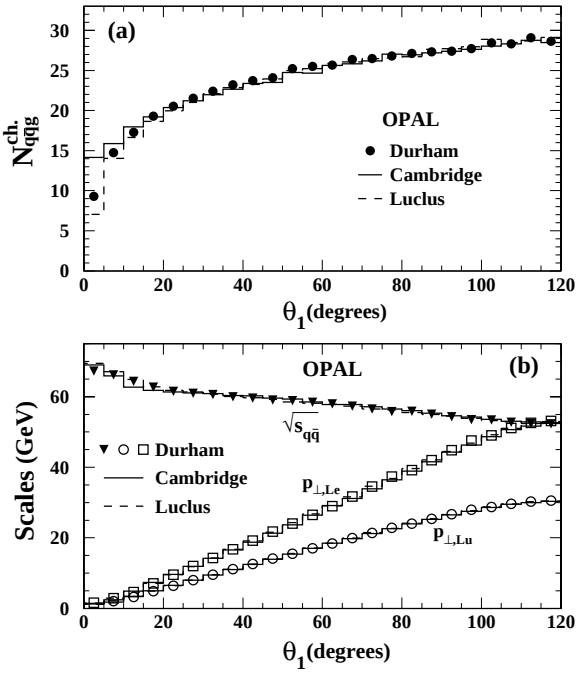

Fig. 3. a Corrected distributions of the mean charged particle multiplicity of three-jet uds flavor Y events from Z^0 decays, selected using the Durham [5], Cambridge [21] and Luclus [6] jet finders, as a function of the opening angle θ_1; **b** the corresponding scales $\sqrt{s_{q\bar{q}}}$, $p_{\perp,Lu}$ and $p_{\perp,Le}$, see (10)–(12). The data have been corrected for initial state photon radiation, detector response, misidentification of uds events, and (for part (b)) misidentification of gluon jets. The uncertainties (too small to be visible) are statistical only

tion of θ_1. $L_{q\bar{q}}$, $k_{\perp,Lu}$ and $k_{\perp,Le}$ are determined using all accepted charged and neutral particles. For the QCD scale parameter Λ, used in the definition of these last three variables (also for the definition of L, see (6)), we choose a value of 0.20 GeV. We verified our results are not sensitive to this choice. Our results for $N^{ch.}_{q\bar{q}g}$ and the corresponding scales $\sqrt{s_{q\bar{q}}}$, $p_{\perp,Lu}$ and $p_{\perp,Le}$ are shown in Fig. 2. The last three variables are obtained from $L_{q\bar{q}}$, $k_{\perp,Lu}$ and $k_{\perp,Le}$ using (7)–(9). We prefer to present $\sqrt{s_{q\bar{q}}}$, $p_{\perp,Lu}$ and $p_{\perp,Le}$ rather than $L_{q\bar{q}}$, $k_{\perp,Lu}$ and $k_{\perp,Le}$ because they provide a clearer illustration of the physical scales in our analysis. The measurements in Fig. 2 are uncorrected and are shown in comparison to the predictions of Jetset at the detector level. By "detector level" we mean the level which includes initial-state radiation, detector simulation, and the same analysis procedures as are applied to the data. Therefore the results in Fig. 2 include the background from non-uds events and gluon jet misidentification, for both the data and simulation.

The measured distributions of $N^{ch.}_{q\bar{q}g}$, $L_{q\bar{q}}$, $k_{\perp,Lu}$ and $k_{\perp,Le}$ are corrected for experimental acceptance and resolution, the effects of initial state photon radiation, and misidentification of uds events, using bin-by-bin multiplicative factors derived from Jetset. The corrections for $L_{q\bar{q}}$, $k_{\perp,Lu}$ and $k_{\perp,Le}$ also account for gluon jet misidentification, i.e. for the contributions of events in which the gluon jet is not jet 3. The data are corrected to the hadron level. The hadron level does not include detector response or initial state radiation and treats all charged and neutral particles with lifetimes greater than 3×10^{-10} s as stable: hence charged particles from the decays of K^0_S and weakly decaying hyperons are included in the corrected distributions. The correction factors are determined as described in [33]. The corrections are typically 1.08 for $N^{ch.}_{q\bar{q}g}$, 0.98 for $L_{q\bar{q}}$, 1.03 for $k_{\perp,Lu}$, and 1.05 for $k_{\perp,Le}$, and do not vary much with θ_1. There is good agreement between the distributions of the uncorrected data and the Monte Carlo sample when the latter includes initial-state radiation and detector simulation, with the same analysis procedures applied to the simulated events as to the data, see Fig. 2.

Corrected distributions of $N^{ch.}_{q\bar{q}g}$, $\sqrt{s_{q\bar{q}}}$, $p_{\perp,Lu}$ and $p_{\perp,Le}$ are shown in Fig. 3. These data are listed in Table 1. Besides the results from our standard analysis, the results found using the Cambridge and Luclus jet finders are shown in Fig. 3. For about 2% of the events, the resolution parameter y_{cut} of the Cambridge algorithm could not be adjusted to yield three reconstructed jets, see [34] for a discussion of this feature of the algorithm. These events were rejected for the Cambridge jet finder based study.

Table 1. Measurements of the mean charged particle multiplicity $N^{ch.}_{q\bar{q}g}$ of three-jet uds flavor Y events from Z^0 decays, as a function of the angle θ_1 between the two lowest energy jets. The jets are defined using the Durham jet-finder. The results for the quark jet scale $\sqrt{s_{q\bar{q}}}$ and the gluon jet scales $p_{\perp,Lu}$ and $p_{\perp,Le}$ are also given. The uncertainties are statistical only. These data are shown in Fig. 3

θ_1 (degrees)	$N^{ch.}_{q\bar{q}g}$	$\sqrt{s_{q\bar{q}}}$ (GeV)	$p_{\perp,Lu}$ (GeV)	$p_{\perp,Le}$ (GeV)
0-5	9.31 ± 0.13	67.27 ± 0.18	1.227 ± 0.007	1.595 ± 0.016
5-10	14.739 ± 0.026	66.182 ± 0.023	2.104 ± 0.003	2.897 ± 0.005
10-15	17.279 ± 0.024	64.385 ± 0.024	3.291 ± 0.003	4.658 ± 0.005
15-20	19.282 ± 0.038	62.679 ± 0.048	4.885 ± 0.005	7.102 ± 0.012
20-25	20.540 ± 0.056	61.530 ± 0.070	6.469 ± 0.009	9.581 ± 0.023
25-30	21.533 ± 0.073	60.945 ± 0.086	8.008 ± 0.013	11.975 ± 0.035
30-35	22.417 ± 0.092	60.597 ± 0.097	9.518 ± 0.017	14.315 ± 0.048
35-40	23.23 ± 0.11	60.02 ± 0.11	11.057 ± 0.022	16.790 ± 0.064
40-45	23.75 ± 0.13	59.61 ± 0.12	12.553 ± 0.027	19.194 ± 0.079
45-50	24.12 ± 0.15	59.04 ± 0.13	14.090 ± 0.033	21.751 ± 0.098
50-55	25.24 ± 0.17	58.88 ± 0.14	15.514 ± 0.038	24.01 ± 0.11
55-60	25.49 ± 0.19	58.45 ± 0.14	16.991 ± 0.043	26.49 ± 0.13
60-65	25.66 ± 0.21	57.94 ± 0.15	18.423 ± 0.049	28.98 ± 0.15
65-70	26.34 ± 0.23	57.32 ± 0.15	19.922 ± 0.055	31.68 ± 0.17
70-75	26.47 ± 0.25	56.55 ± 0.16	21.443 ± 0.061	34.56 ± 0.19
75-80	26.79 ± 0.26	55.81 ± 0.16	22.879 ± 0.065	37.36 ± 0.21
80-85	27.10 ± 0.28	55.89 ± 0.14	24.018 ± 0.064	39.21 ± 0.20
85-90	27.29 ± 0.31	55.04 ± 0.14	25.388 ± 0.065	42.04 ± 0.21
90-95	27.37 ± 0.31	54.29 ± 0.13	26.687 ± 0.066	44.80 ± 0.22
95-100	27.72 ± 0.33	53.48 ± 0.12	27.927 ± 0.065	47.59 ± 0.22
100-105	28.42 ± 0.36	53.384 ± 0.097	28.703 ± 0.054	49.00 ± 0.18
105-110	28.31 ± 0.35	52.779 ± 0.077	29.620 ± 0.046	51.15 ± 0.15
110-115	29.08 ± 0.36	52.416 ± 0.053	30.240 ± 0.032	52.58 ± 0.11
115-120	28.62 ± 0.37	52.328 ± 0.032	30.497 ± 0.020	53.115 ± 0.066

We invert (4) and (5) to obtain expressions for the unbiased gluon jet charged particle multiplicities $N^{ch.}_{gg}(k_\perp)$:

$$N^{ch.}_{gg}(k_{\perp,Lu}(\theta_1)) = 2\left[N^{ch.}_{q\bar{q}g}(L,\theta_1) - N^{ch.}_{q\bar{q}}(L,k_{\perp,Lu}(\theta_1))\right], \quad (15)$$

$$N^{ch.}_{gg}(k_{\perp,Le}(\theta_1)) = 2\left[N^{ch.}_{q\bar{q}g}(L,\theta_1) - N^{ch.}_{q\bar{q}}(L_{q\bar{q}}(\theta_1),k_{\perp,Lu}(\theta_1))\right], \quad (16)$$

where $N^{ch.}_{q\bar{q}g}$, $L_{q\bar{q}}$, $k_{\perp,Lu}$ and $k_{\perp,Le}$ are determined from the Y events as described above.

To find the $N^{ch.}_{q\bar{q}}(L,k_{\perp,Lu})$ terms in (15), we employ two methods. First, for the standard analysis, we perform a direct measurement. Specifically we determine the particle multiplicity of two-jet uds events from Z^0 decays (i.e. at a fixed value of L corresponding to $E_{c.m.} = 91.2$ GeV) as a function of the jet resolution scale $k_{\perp,Lu}$. This result is presented in Sect. 6.1. Second, as a systematic check (see Sect. 7), we evaluate the analytic expression, (13), as explained in the following paragraph. To find the $N^{ch.}_{q\bar{q}}(L_{q\bar{q}},k_{\perp,Lu})$ terms in (16), we utilize only the second of these methods, i.e. the one based on (13). A direct measurement is not straightforward in this case because $L_{q\bar{q}}$, unlike L, is a variable quantity. A direct measurement of $N^{ch.}_{q\bar{q}}(L_{q\bar{q}},k_{\perp,Lu})$ at the scales relevant for our analysis would in principle require a determination of the particle multiplicity in two-jet events as a function of $p_{\perp,Lu}$ for c.m. energies below the Z^0. So far, no such measurements are available.

Our procedure to determine $N^{ch.}_{q\bar{q}}(J,k_{\perp,Lu})$ in (15) and (16) using the analytic expression, (13), is as follows. We begin with the compilation of the mean charged particle multiplicity of e^+e^- hadronic annihilations, $N^{ch.}_{e^+e^-}$ versus $E_{c.m.}$, given in [12]. These data are shown as a function of $E_{c.m.}$ by the open symbols in Fig. 4. (For simplicity, not all the LEP-averaged results compiled in [12] are displayed in Fig. 4; however, these data are included in the procedure described below.) We correct these results for the contributions of c and b events so they correspond to our treatment of $N^{ch.}_{q\bar{q}g}$ as explained in Sect. 4, i.e. to uds events only. This correction is a bin-by-bin multiplicative factor determined from Jetset, given by the ratio of $N^{ch.}_{e^+e^-}$ between uds and udscb events as a function of $E_{c.m.}$. Jetset has been found to provide an accurate description of the multiplicity of both the uds flavor and flavor inclusive samples in e^+e^- hadronic annihilations (see for ex-

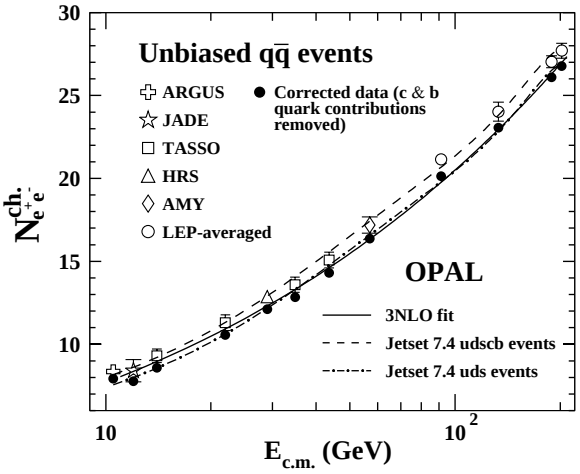

Fig. 4. Measurements (see [12] for the original references) of the inclusive charged particle multiplicity in e^+e^- annihilations (open symbols) as a function of $E_{c.m.}$. The LEP results are averages over the LEP experiments (see [12]). The solid points show the corresponding results after corrections to remove the contributions of c and b events. For simplicity the uncertainties of the corrected data are not shown: these are essentially the same as those of the corresponding uncorrected data points. The solid curve is a fit of the next-to-next-to-next-to-leading order (3NLO) expression for quark jet multiplicity [14,36] to the corrected data. The predictions of the Jetset event generator for udscb and uds flavor events are also shown

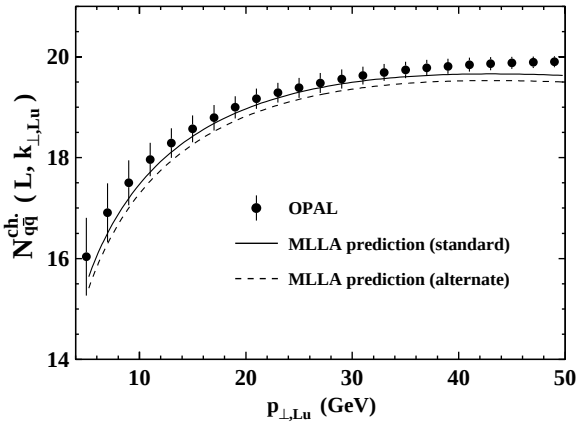

Fig. 5. The mean charged particle multiplicity of biased two-jet uds flavor events from Z^0 decays selected using the Durham jet finder. The results are presented as a function of $p_{\perp,Lu}$, related to the resolution parameter y_{cut} of the jet finder by $p_{\perp,Lu} = E_{vis.}\sqrt{y_{cut}}$ with $E_{vis.}$ the event energy. The data have been corrected for initial state photon radiation, detector response, and misidentification of uds events. The uncertainties are the statistical and systematic terms added in quadrature. The statistical uncertainties are smaller than the symbol sizes. The solid curve shows the prediction [15] of the modified leading logarithmic approximation (MLLA) expression, (13). The prediction is seem to agree with the data up to scales of about 40 GeV. The dashed curve is the MLLA result found by altering the choice of data points used in the fit of $N^{ch.}_{e^+e^-}$ versus scale

ample [9,10,35]), justifying its use for this correction. The predictions of Jetset for $N^{ch.}_{e^+e^-}$ in udscb and uds flavor events are shown by the dashed and dash-dotted curves in Fig. 4. The correction factors have values between 0.92 and 0.96. The corrected results for $N^{ch.}_{e^+e^-}$, corresponding to the terms $N_{q\bar{q}}(J')$ in (13) and which we denote $N^{ch.}_{q\bar{q}}(L)$ in the following, are shown by the solid points in Fig. 4. We fit these corrected data using the next-to-next-to-next-to-leading order (3NLO) analytic expression for the scale dependence of quark jet multiplicity N_q [14,36] assuming $n_f = 5$. Two parameters are fitted: an effective QCD scale parameter, $\Lambda_{eff.}$, and an overall normalization constant, K. The fit results are given in the first row of Table 2. The result of the fit is shown by the solid curve in Fig. 4. Using this fitted curve and its derivative, we numerically evaluate (13) as a function of θ_1 to determine the biased quark terms $N^{ch.}_{q\bar{q}}(J, k_{\perp,Lu})$ in (15) and (16). The derivative is evaluated by differentiating the analytic expression for N_q with respect to $y = L/2$ and using the fitted parameter values for $N^{ch.}_{q\bar{q}}(L)$ from Table 2.

Table 2. Results of fits of the 3NLO expressions for quark and gluon jet multiplicities to measurements of charged particle multiplicity in unbiased $q\bar{q}$ and gg events, see the solid curves in Figs. 4 and 6a. The fits are performed assuming five active quark flavors. The uncertainties are statistical only. The χ^2 per degree-of-freedom (d.o.f.) of the fits are also given. The χ^2 values are determined using the statistical uncertainties of the data and not the systematic terms

	$\Lambda_{eff.}$ (GeV)	Normalization K	χ^2 (d.o.f.)
$N^{ch.}_{q\bar{q}}(L)$, uds quark jets	0.190 ± 0.032	0.136 ± 0.009	6.1 (16)
$N^{ch.}_{gg}(L)$, gluon jets	0.600 ± 0.059	0.201 ± 0.011	28.1 (17)

6 Results

6.1 The biased quark jet multiplicities $N^{ch.}_{q\bar{q}}(J, k_{\perp,Lu})$

In this section we present our direct measurement of the biased quark jet terms $N^{ch.}_{q\bar{q}}(L, k_{\perp,Lu})$ in (15). We then use these data to test the analytic expression, (13).

We apply the Durham jet finder to the sample of uds flavor events described in Sect. 4 using a fixed value of the resolution parameter y_{cut} (see below). Events are retained if exactly two jets are reconstructed. The solid points in Fig. 5 show the charged particle multiplicity of the selected two-jet events for different choices of y_{cut}. We relate y_{cut} to the transverse momentum $p_{\perp,Lu}$ through $p_{\perp,Lu} = E_{vis.}\sqrt{y_{cut}}$ [16], with $E_{vis.}$ the sum of the particle energy in the event. The data are corrected for initial state radiation, the effects of the detector, and uds event misidentification, and are plotted as a function of $p_{\perp,Lu}$. The solid points in Fig. 5 therefore represent the direct measurements of the biased quark jet terms $N^{ch.}_{q\bar{q}}(L, k_{\perp,Lu})$ mentioned in Sect. 5. The vertical lines show the total uncertainties, with statistical and systematic terms added in

Table 3. Measurements of the mean charged particle multiplicity of biased two-jet uds flavor events from Z^0 decays as a function of the transverse momentum cutoff $p_{\perp,Lu}$ used to separate two- and three-jet events. The jets are defined using the Durham jet-finder. The first uncertainty is statistical and the second systematic. These data are shown in Fig. 5

$p_{\perp,Lu}$ (GeV)	$N^{ch.}_{q\bar{q}}(L, k_{\perp,Lu})$	$p_{\perp,Lu}$ (GeV)	$N^{ch.}_{q\bar{q}}(L, k_{\perp,Lu})$
5.0	$16.04 \pm 0.04 \pm 0.77$	29.0	$19.56 \pm 0.04 \pm 0.19$
7.0	$16.91 \pm 0.04 \pm 0.58$	31.0	$19.63 \pm 0.04 \pm 0.17$
9.0	$17.50 \pm 0.04 \pm 0.44$	33.0	$19.69 \pm 0.04 \pm 0.16$
11.0	$17.96 \pm 0.04 \pm 0.33$	35.0	$19.74 \pm 0.04 \pm 0.16$
13.0	$18.29 \pm 0.04 \pm 0.29$	37.0	$19.78 \pm 0.04 \pm 0.15$
15.0	$18.57 \pm 0.04 \pm 0.26$	39.0	$19.81 \pm 0.04 \pm 0.14$
17.0	$18.79 \pm 0.04 \pm 0.25$	41.0	$19.84 \pm 0.04 \pm 0.13$
19.0	$19.00 \pm 0.04 \pm 0.21$	43.0	$19.86 \pm 0.04 \pm 0.13$
21.0	$19.17 \pm 0.04 \pm 0.20$	45.0	$19.88 \pm 0.04 \pm 0.12$
23.0	$19.29 \pm 0.04 \pm 0.19$	47.0	$19.89 \pm 0.04 \pm 0.11$
25.0	$19.38 \pm 0.04 \pm 0.19$	49.0	$19.90 \pm 0.04 \pm 0.10$
27.0	$19.48 \pm 0.04 \pm 0.19$		

quadrature. The evaluation of systematic uncertainties is discussed in Sect. 7. The statistical uncertainties are negligible compared to the systematic terms. These data are listed in Table 3. As part of our evaluation of systematic uncertainties, results analogous to those shown in Fig. 5 are determined using the Cambridge jet finder. For the Cambridge algorithm, the resolution parameter y_{cut} is related to $p_{\perp,Lu}$ by the expression given above. We do not determine analogous results using the Luclus jet finder because it is not obvious how to relate the resolution parameter d_{join} to $p_{\perp,Lu}$ in this case.

The solid curve in Fig. 5 shows the prediction for $N^{ch.}_{q\bar{q}}(L, k_{\perp,Lu})$ found using (13), evaluated as explained in Sect. 5. The curve is seen to describe the direct measurements fairly well. In particular, the shape of the analytic curve is generally similar to the data, at least for values of scale below about 40 GeV. This suggests that the MLLA result, (13), is adequate for the purposes of our study. We return to this question in Sect. 6.2.

The difference between the results found using the Durham and Cambridge jet finders is the dominant source of systematic uncertainty for the data in Fig. 5 (Sect. 7). The results from the Durham algorithm (standard analysis) lie closer to the MLLA curve than those from the Cambridge algorithm, especially for small values of θ_1.

As a systematic check of the MLLA prediction for $N^{ch.}_{q\bar{q}}(L, k_{\perp,Lu})$, we re-evaluated the prediction after excluding the ARGUS and 91 GeV LEP measurements from the fit of $N^{ch.}_{e^+e^-}$ versus $E_{c.m.}$ (see Fig. 4). More details are given in Sect. 7. This alternate result is shown by the dashed curve in Fig. 5. The difference between the solid and dashed curves is seen to be similar to the difference between the solid curve and symbols. This suggests that the agreement of the analytic expression (13) with the direct measurements is quite reasonable, once sources of systematic uncertainty are considered.

6.2 Unbiased gluon jet multiplicity versus scale

Figure 6 shows our results for the unbiased charged particle multiplicities of gg events, $N^{ch.}_{gg}$. The solid points in Fig. 6a are obtained from (15) using the direct measurements of $N^{ch.}_{q\bar{q}}(L, k_{\perp,Lu})$, i.e. the solid points in Fig. 5[6]. The small horizontal bars indicate the statistical uncertainties. The vertical lines show the total uncertainties, with statistical and systematic terms added in quadrature. The evaluation of systematic uncertainties is discussed in Sect. 7. The asterisks and open symbols in Fig. 6b show the corresponding results from (15) and (16) using the calculated expressions for $N^{ch.}_{q\bar{q}}(J, k_{\perp,Lu})$ from (13). Thus the asterisks in Fig. 6b are derived using the solid curve in Fig. 5, for example. The two sets of results from (15) (solid points in Fig. 6a and asterisks in Fig. 6b) are seen to be very similar. This is consistent with the observation in Sect. 6.1 that (13) is generally adequate for the purposes of our study.

The results from (15) are plotted as a function of $Q = p_{\perp,Lu}$ and those from (16) as a function of $Q = p_{\perp,Le}$. The variable $p_{\perp,Lu}$ extends over a smaller range of scale than $p_{\perp,Le}$ because the factor of s in the denominator of the Lund definition of transverse momentum is always larger in Y events than the factor of $s_{q\bar{q}}$ in the Leningrad definition, see (11) and (12). This effect is also visible in Fig. 3b and Table 1, i.e. $p_{\perp,Lu}$ has a maximum of 30.5 GeV compared to 53.1 GeV for $p_{\perp,Le}$. Note that with $\theta_1 \geq 35^\circ$ as in our standard analysis, the lower bound on the gluon jet scale is 11.1 GeV for $p_{\perp,Lu}$ and 16.8 GeV for $p_{\perp,Le}$, see Fig. 3b.

Included in Fig. 6 are direct measurements of the inclusive charged particle multiplicity of unbiased gluon jets from the CLEO and OPAL Collaborations, currently the only results which utilize a hemisphere definition of gluon jets. These results are shown by the triangular symbols. The three data points at scales of about 4-7 GeV are derived from the hadronic component of $\Upsilon(1S) \to \gamma gg$ events [8]. The scale Q for these data is given by the invariant mass of the hadronic system. Similarly, $\Upsilon(3S) \to \gamma\chi_{b2}(2P) \to \gamma gg$ events provide the result at $Q = 10.3$ GeV [7], with the scale given by the $\chi_{b2}(2P)$ mass. The measurement at $Q = 80.2$ GeV [11] is determined using hadronic Z^0 decays: $Z^0 \to q\bar{q}g_{incl.}$, where $g_{incl.}$ refers to a gluon jet hemisphere recoiling against two almost collinear identified quark jets q and $\bar{q}$ in the opposite hemisphere [37]. For our purposes the $g_{incl.}$ measurement from [11] has been multiplied by a factor of two both for the multiplicity and energy scale so it corresponds to gg "two-jet events" analogous to the other data in Fig. 6.

[6] We parametrize the data in Fig. 5 using a polynomial. We then evaluate this polynomial at the scale values corresponding to our bins in θ_1 (see Table 1) to determine the gluon jet multiplicities using (15)

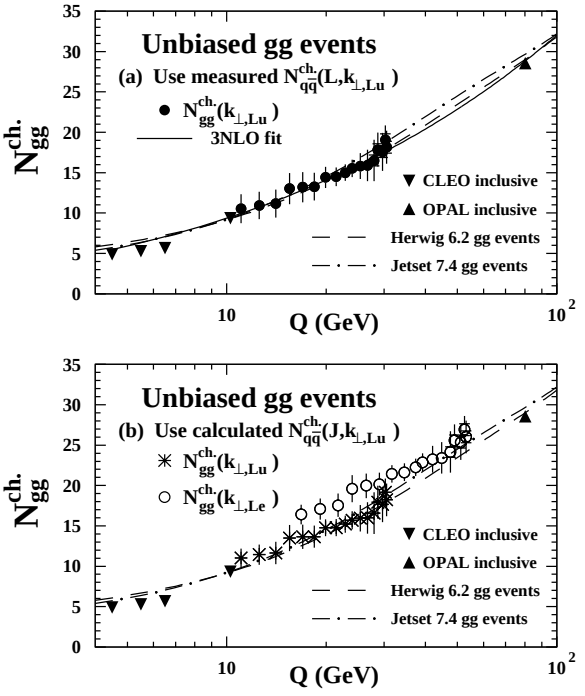

Fig. 6a,b. The mean charged particle multiplicity of unbiased gg events as a function of scale. **a** Results from (15) using the measured biased quark jet terms $N^{ch.}_{q\bar{q}}(L,k_{\perp,Lu})$. The small horizontal bars indicate the statistical uncertainties. The vertical lines show the total uncertainties, with statistical and systematic terms added in quadrature. The solid curve is a fit of the 3NLO expression for gluon jet multiplicity [14,36] to the data. **b** The corresponding results from (15) and (16) using the MLLA expression for the biased quark jet terms $N^{ch.}_{q\bar{q}}(J,k_{\perp,Lu})$, (13), where $J=L$ for the $N^{ch.}_{gg}(k_{\perp,Lu})$ results and $J=L_{q\bar{q}}$ for the $N^{ch.}_{gg}(k_{\perp,Le})$ results. For both **a** and **b**, the triangles show measurements of the inclusive charged particle multiplicity of unbiased gluon jets from the CLEO [7,8] and OPAL [11] Collaborations. The predictions of the Herwig and Jetset Monte Carlo event generators are also shown

Figure 6 also shows the predictions of the Herwig [38, 39] and Jetset Monte Carlo event generators for the inclusive charged particle multiplicity of gg events versus $Q=E_{c.m.}$. For these results we use version 6.2 [39] of Herwig with the following changes to the default parameter set: the parameter specifying the angular smearing of udsc quark clusters, CLSMR(1), is set to 0.40, the parameter controlling the mass spectrum of b quark clusters, PSPLT(2), is set to 0.33, and the parameter controlling the production of decuplet baryons, DECWT, is set to 0.70. Herwig 6.2 with these changes is found to provide a good description of the global features of the OPAL data including those of flavor selected samples.

From Fig. 6 it is seen that the Monte Carlo predictions describe the direct measurements of unbiased gluon jet multiplicity (triangle symbols) well. The results from the present analysis based on (15) (solid points in Fig. 6a and asterisks in Fig. 6b) are also well described by the Monte Carlo curves. In contrast, the results from (16) (open symbols in Fig. 6b) are generally well above the Monte Carlo predictions, and – if extrapolated to lower and higher energies – appear inconsistent with the direct measurements from CLEO and OPAL as well. We note that both Jetset and Herwig have been found to provide a good description of gluon jet properties, including multiplicity, in other studies (see for example [2]- [4], [11], [40]). We therefore conclude that the equation based on the Lund definition of the gluon jet scale, (4), yields results which are more consistent with other studies than the equation based on the Leningrad definition, (5). Our data thus allow a fairly clear discrimination between (4) and (5). We henceforth restrict our analysis of gluon jets to the former set of results. Numerical values for the gluon jet measurements based on (4) (and (15)) are presented in Table 4. The analogous

Table 4. Measurements of unbiased gluon jet multiplicity $N^{ch.}_{gg}$ as a function of energy scale $Q=p_{\perp,Lu}$, obtained using (15). The corresponding bins of θ_1 in Y events are also indicated. The results for $\theta_1 \geq 35^\circ$, listed in the bottom part of the table, are used in our standard analysis. These data are shown by the solid points in Fig. 6a. For information, we also list the results obtained for smaller values of θ_1. Note that the theoretical formalism used to determine these results is not expected to be valid for small θ_1. This explains the negative value of multiplicity derived for $\theta_1 < 5^\circ$. The corresponding results for the multiplicity ratio r between gluon and quark jets are also given. The results for r for $\theta_1 \geq 35^\circ$ are shown by the solid points in Figs. 7 and 9a

Q (GeV)	θ_1 (degrees)	$N^{ch.}_{gg}(k_{\perp,Lu})$	r
1.23	0-5	$-8.8 \pm 0.3 \pm 6.4$	$-3.1 \pm 0.1 \pm 2.1$
2.10	5-10	$0.9 \pm 0.1 \pm 4.8$	$0.3 \pm 0.0 \pm 1.5$
3.29	10-15	$4.6 \pm 0.1 \pm 2.4$	$1.00 \pm 0.01 \pm 0.56$
4.88	15-20	$6.9 \pm 0.1 \pm 1.8$	$1.25 \pm 0.01 \pm 0.34$
6.47	20-25	$8.0 \pm 0.1 \pm 1.9$	$1.28 \pm 0.02 \pm 0.31$
8.01	25-30	$8.9 \pm 0.2 \pm 1.9$	$1.28 \pm 0.02 \pm 0.27$
9.52	30-35	$9.7 \pm 0.2 \pm 1.9$	$1.29 \pm 0.02 \pm 0.26$
11.1	35-40	$10.6 \pm 0.2 \pm 1.8$	$1.31 \pm 0.03 \pm 0.22$
12.6	40-45	$11.0 \pm 0.3 \pm 1.7$	$1.29 \pm 0.03 \pm 0.20$
14.1	45-50	$11.2 \pm 0.3 \pm 1.7$	$1.25 \pm 0.03 \pm 0.19$
15.5	50-55	$13.0 \pm 0.3 \pm 1.9$	$1.39 \pm 0.04 \pm 0.20$
17.0	55-60	$13.2 \pm 0.4 \pm 1.8$	$1.35 \pm 0.04 \pm 0.19$
18.4	60-65	$13.3 \pm 0.4 \pm 1.7$	$1.31 \pm 0.04 \pm 0.17$
19.9	65-70	$14.4 \pm 0.5 \pm 1.2$	$1.38 \pm 0.05 \pm 0.12$
21.4	70-75	$14.5 \pm 0.5 \pm 1.1$	$1.344 \pm 0.046 \pm 0.098$
22.9	75-80	$15.00 \pm 0.52 \pm 0.87$	$1.353 \pm 0.047 \pm 0.079$
24.0	80-85	$15.53 \pm 0.57 \pm 0.94$	$1.371 \pm 0.050 \pm 0.083$
25.4	85-90	$15.8 \pm 0.6 \pm 1.5$	$1.36 \pm 0.05 \pm 0.13$
26.7	90-95	$15.9 \pm 0.6 \pm 1.9$	$1.34 \pm 0.05 \pm 0.16$
27.9	95-100	$16.5 \pm 0.7 \pm 2.5$	$1.37 \pm 0.06 \pm 0.21$
28.7	100-105	$17.9 \pm 0.7 \pm 2.0$	$1.46 \pm 0.06 \pm 0.16$
29.6	105-110	$17.6 \pm 0.7 \pm 2.3$	$1.42 \pm 0.06 \pm 0.18$
30.2	110-115	$19.1 \pm 0.7 \pm 1.6$	$1.53 \pm 0.06 \pm 0.13$
30.5	115-120	$18.2 \pm 0.7 \pm 1.9$	$1.45 \pm 0.06 \pm 0.15$

Table 5. Measurements of unbiased gluon jet multiplicity $N_{gg}^{ch.}$ as a function of energy scale $Q = p_{\perp,Le}$, obtained using (16). Note that the theoretical formalism used to determine these results is not expected to be valid for small θ_1. This explains the negative value of multiplicity derived for $\theta_1 < 5^\circ$. The results corresponding to $\theta_1 \geq 35^\circ$ are shown by the open points in Fig. 6b

Q (GeV)	θ_1 (degrees)	$N_{gg}^{ch.}$ $(k_{\perp,Le})$
1.59	0-5	$-1.2 \pm 0.3 \pm 6.5$
2.90	5-10	$6.8 \pm 0.1 \pm 4.8$
4.66	10-15	$9.5 \pm 0.1 \pm 2.1$
7.10	15-20	$11.6 \pm 0.1 \pm 1.5$
9.58	20-25	$12.9 \pm 0.1 \pm 1.5$
12.0	25-30	$14.1 \pm 0.2 \pm 1.3$
14.3	30-35	$15.2 \pm 0.2 \pm 1.2$
16.8	35-40	$16.4 \pm 0.2 \pm 1.2$
19.2	40-45	$17.1 \pm 0.3 \pm 1.3$
21.8	45-50	$17.6 \pm 0.3 \pm 1.4$
24.0	50-55	$19.6 \pm 0.3 \pm 1.7$
26.5	55-60	$20.0 \pm 0.4 \pm 1.5$
29.0	60-65	$20.2 \pm 0.4 \pm 1.4$
31.7	65-70	$21.44 \pm 0.47 \pm 0.99$
34.6	70-75	$21.65 \pm 0.49 \pm 0.99$
37.4	75-80	$22.25 \pm 0.52 \pm 0.95$
39.2	80-85	$22.86 \pm 0.57 \pm 0.96$
42.0	85-90	$23.3 \pm 0.6 \pm 1.5$
44.8	90-95	$23.4 \pm 0.6 \pm 1.8$
47.6	95-100	$24.1 \pm 0.7 \pm 2.5$
49.0	100-105	$25.6 \pm 0.7 \pm 1.9$
51.1	105-110	$25.4 \pm 0.7 \pm 2.1$
52.6	110-115	$26.9 \pm 0.7 \pm 1.6$
53.1	115-120	$26.0 \pm 0.7 \pm 1.9$

results based on (5) (and (16)) are presented in Table 5. For information, we include results corresponding to all θ_1 bins in these tables, not just the bins above 35° used in our standard analysis. Note that the theoretical formalism is not expected to be valid for small values of θ_1. This explains the negative values of multiplicity determined for the first bin, $0 \leq \theta_1 \leq 5^\circ$.

6.3 The ratios r, $r^{(1)}$ and $r^{(2)}$

6.3.1 Determination of the ratios

Having established that the formalism of [15] yields consistent results with the direct measurements of unbiased gluon jet multiplicity if the equation for three-jet event multiplicity based on the Lund definition of transverse momentum is employed (Sect. 6.2), we proceed to a comparison of the unbiased gluon and quark jet terms and to a test of the theoretical expressions for the ratios r, $r^{(1)}$ and $r^{(2)}$, see (1)–(3). For this purpose we use the gluon jet data

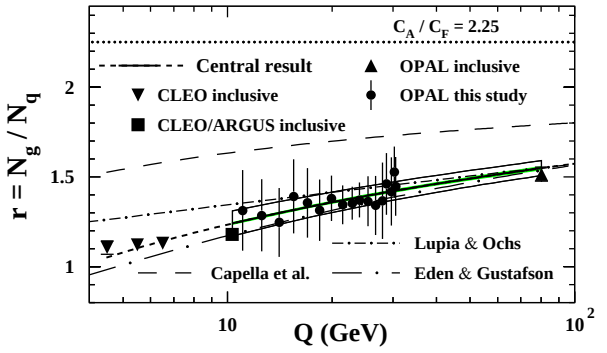

Fig. 7. Results for the ratio r of the mean charged particle multiplicities between unbiased gluon and uds quark jets as a function of scale. The central result is shown by the solid curve; the shaded and open bands show the corresponding statistical and total uncertainties, respectively (the statistical uncertainties are barely visible). The short-dashed curve is an extrapolation of the fit. The solid points show measurements based on gluon jet results from the present analysis. The triangle and square symbols show results based on direct measurements of multiplicity in unbiased jets from the CLEO [7,8], ARGUS [41] and OPAL [11] Collaborations. The dash-dotted and long-dashed curves show theoretical predictions based on analytic [14,15] and numerical [13] techniques

shown by the solid points in Fig. 6a since these results are derived using the direct measurements of $N_{q\bar{q}}^{ch.}$ $(L, k_{\perp,Lu})$ rather than the MLLA expression, (13). They therefore rely on fewer theoretical assumptions.

We employ the following procedure to determine r, $r^{(1)}$ and $r^{(2)}$ from experiment. The corrected unbiased quark and gluon jet multiplicities, shown by the solid points in Figs. 4 and 6a, are separately fitted using the 3NLO expressions for N_q and N_g [14,36], respectively. To better constrain the results, the measurements of inclusive gluon jet multiplicity from CLEO at 10.3 GeV and OPAL at 80.2 GeV are included in the gluon jet fit. The fitted parameters are $\Lambda_{eff.}$ and the normalization constant K. (For the quark jet data, this is the same fit discussed in Sect. 5.) The results of the fits are shown by the solid curves in Figs. 4 and 6a. The fitted parameters and corresponding χ^2 per degree-of-freedom are listed in Table 2. The χ^2 per d.o.f. and overall description of the data are seen to be reasonable in both cases. The ratio of the fitted expressions for N_g and N_q defines r, (1). We calculate the first and second derivatives of the analytic equations for N_g and N_q with respect to y and evaluate the resulting expressions using the corresponding parameter values from Table 2. The ratios of these terms define $r^{(1)}$ and $r^{(2)}$, (2) and (3).

Our results for r are shown in Fig. 7, and those for $r^{(1)}$ and $r^{(2)}$ in Fig. 8. The central results are indicated by solid curves. The shaded bands show the statistical uncertainties. The overall uncertainties, with statistical and systematic terms added in quadrature, are shown by the open bands. The bands cover the energy range of data in the gluon jet fit, from 10.3 to 80.2 GeV. The short-dashed curves show extrapolations of the results to lower

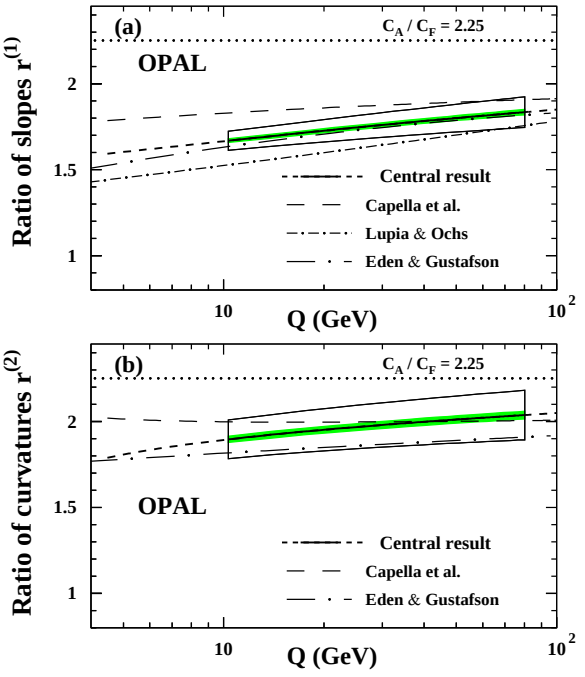

Fig. 8a,b. The ratios of slopes $r^{(1)}$ and of curvatures $r^{(2)}$ between unbiased gluon and uds quark jets as a function of scale. The curves and bands have the same meaning as in Fig. 7

and higher scales. At 30 GeV, a typical scale for the gluon jet data in these figures, the ratios are determined to be:

$$r\,(30\,GeV) = 1.422 \pm 0.006 \pm 0.051 \quad , \qquad (17)$$

$$r^{(1)}\,(30\,GeV) = 1.761 \pm 0.013 \pm 0.070 \quad , \qquad (18)$$

$$r^{(2)}\,(30\,GeV) = 1.98 \pm 0.02 \pm 0.13 \quad , \qquad (19)$$

where the first uncertainty is statistical and the second systematic. At 80 GeV, corresponding to the highest energy gluon jet data in the fits, the results are:

$$r\,(80\,GeV) = 1.548 \pm 0.008 \pm 0.041 \quad , \qquad (20)$$

$$r^{(1)}\,(80\,GeV) = 1.834 \pm 0.016 \pm 0.088 \quad , \qquad (21)$$

$$r^{(2)}\,(80\,GeV) = 2.04 \pm 0.02 \pm 0.14 \quad . \qquad (22)$$

Analogous results for r versus scale were previously published in [4,18,19] and for $r^{(1)}$ in [18,19]. These earlier studies were based on biased jet samples, however. Therefore the quantitative results from those studies cannot be compared to theoretical predictions without ambiguity. Our result for $r^{(2)}$ is the first experimental determination of that quantity.

Included in Fig. 7 are the results for r derived from the individual gluon jet measurements in Fig. 6a. The solid points in Fig. 7 are obtained by dividing the results shown by the solid points in Fig. 6a by the results of the 3NLO parametrization of quark jet multiplicity at the corresponding scales. Numerical values of these results for r are compiled in Table 4. The triangle and square symbols in Fig. 7 are obtained as follows: (i) for the OPAL data point at 80.2 GeV, the published result [11] is used, based on uds quark events analogous to the present study; (ii) for the three CLEO points at 4-7 GeV, the published results [8] are used after applying a correction obtained from Jetset to remove the contributions of c events from the quark jet samples; (iii) for the point labelled "CLEO/ARGUS," the CLEO measurement of gluon jet multiplicity at 10.3 GeV [7] is divided by the ARGUS measurement of $N^{ch.}_{e^+e^-}$ at 10.5 GeV [41] (see Fig. 4), after applying a correction to account for c and b events in the quark jet sample and for the small energy difference between the gluon and quark jet results.

As a consistency check, we also determined the ratios r and $r^{(1)}$ using the technique employed in [19]. The corrected quark jet results (solid points in Fig. 4) were fitted using a polynomial expression:

$$N_{q\bar{q}} = a_0 + a_1\,L + a_2\,L^2 \quad , \qquad (23)$$

with L given in (6), and where a_0, a_1 and a_2 are fitted parameters. We find $a_0 = 13.20 \pm 0.67$, $a_1 = -2.91 \pm 0.12$ and $a_2 = 0.2818 \pm 0.0057$, where the uncertainties are statistical. The χ^2 (d.o.f.) of the fit is 3.74 (15). We then fitted the 19 gluon jet measurements in our analysis (solid points in Fig. 6a and the 10.3 and 80.2 GeV results from CLEO and OPAL) using the expression:

$$N_{gg} = b_0 + b_1\,N_{q\bar{q}} \quad , \qquad (24)$$

with the results $b_0 = -4.07 \pm 0.27$, $b_1 = 1.759 \pm 0.030$ and χ^2 (d.o.f.) $= 31.5$ (17). The result for r, given by the ratio of (24) and (23), is indistinguishable from the solid curve in Fig. 7. The result for $r^{(1)}$, obtained by differentiation of (24), is, by construction, a constant: $r^{(1)} \equiv b_1 = 1.759 \pm 0.030$ (stat.). This result is consistent with that shown in Fig. 8a, see also (18). Not only is $r^{(1)}$ constant with this method, but $r^{(2)} \equiv b_1 = r^{(1)}$, i.e. no distinction is made between the ratios of slopes and curvatures. Therefore this alternate technique does not provide as much information as our standard procedure described above.

To obtain a consistency check of our result for $r^{(2)}$, we applied the following procedure. The 19 gluon jet measurements were clustered into 16 groups of four contiguous measurements. Thus, labelling the data points from 1 to 19 in order of increasing Q, the first group is composed of data points 1-4, the second of 2-5, etc. A straight line fit was performed for each group:

$$(N_{gg})_i = (a_g)_i\,L + (b_g)_i \qquad i = 1, 16 \quad , \qquad (25)$$

with a_g and b_g the fitted parameters. By fitting to four points at a time, rather than e.g. to two points only, the influence of bin-to-bin fluctuations is reduced. We then evaluated the fitted polynomial expression (23) at the scale values of the gluon jet measurements to obtain 19 corresponding results for quark jets, which were then fitted in the same manner:

$$(N_{q\bar{q}})_i = (a_q)_i\,L + (b_q)_i \qquad i = 1, 16 \quad . \qquad (26)$$

A scale value was associated with each slope point $(a_g)_i$ or $(a_q)_i$ using the arithmetic mean of the four Q values

in the fits. As a systematic check, we also defined these scales using the weighted means of the Q values of the four associated gluon jet measurements. This alternate method yielded consistent results with those presented below. The slopes $(a_g)_i$ and $(a_q)_i$ were in turn fitted using straight lines:

$$a_g = c_g\, L + d_g \tag{27}$$

$$a_q = c_q\, L + d_q \tag{28}$$

with c_i and d_i $(i = q, g)$ the fitted terms. The ratio $r^{(2)}$ found using this technique is a constant given by $r^{(2)} = c_g/c_q$. We find $r^{(2)} = 2.25 \pm 0.16\,(\text{stat.})$, consistent with our result in Fig. 8b, see also (19).

The procedure described in the previous paragraph can also be used to obtain a second consistency check for $r^{(1)}$. Taking the weighted mean of the 16 results for the ratio of slopes $r_i^{(1)} = (a_g/a_q)_i$ yields $r^{(1)} = 1.68 \pm 0.02\,(\text{stat.})$, consistent with the result in (18) to within about 1.0 standard deviation of the total uncertainties.

We note that the method to determine $r^{(1)}$ and $r^{(2)}$ based on (25)–(28) is more direct than our standard procedure because no functional form is assumed for how the gluon jet multiplicity varies with scale. The resulting uncertainties are considerably larger, however, and no information on the scale dependence of $r^{(1)}$ and $r^{(2)}$ is obtained. Therefore we retain the analysis based on the 3NLO parametrizations of multiplicities for our standard results.

Analytic expressions for r, $r^{(1)}$ and $r^{(2)}$, valid to 3NLO, were recently presented by Capella et al. [14]. All three ratios are predicted to converge to the ratio of QCD color factors, $C_A/C_F = 2.25$, in the asymptotic limit of large jet energies. This convergence is predicted to be more rapid for $r^{(1)}$ than r [14,18] and yet more rapid for $r^{(2)}$ [14]. Our data are in agreement with this prediction, i.e. $r < r^{(1)} < r^{(2)} < 2.25$ for the scales accessible in our study, see (17)–(22). Note that we also observe the hierarchy $r < r^{(1)} < r^{(2)}$ using the alternate analysis strategies summarized by (23)–(28).

To make the comparison of our results for r, $r^{(1)}$ and $r^{(2)}$ more clear, the data from Figs. 7 and 8 are displayed together in Fig. 9a. The dominant uncertainties in our analysis are systematic (see Sect. 7) and are correlated between the three ratios. Therefore, in Fig. 9b, we present results for the differences $r^{(2)} - r$, $r^{(1)} - r$ and $r^{(2)} - r^{(1)}$, for which correlated systematic uncertainties partially cancel. At 30 GeV, we find:

$$\left[r^{(2)} - r\right]\,(30\,GeV) = 0.56 \pm 0.02 \pm 0.14 \quad , \tag{29}$$

$$\left[r^{(1)} - r\right]\,(30\,GeV) = 0.341 \pm 0.014 \pm 0.075 \quad , \tag{30}$$

$$\left[r^{(2)} - r^{(1)}\right]\,(30\,GeV) = 0.221 \pm 0.024 \pm 0.070 \quad , \tag{31}$$

where the first uncertainty is statistical and the second systematic. These results demonstrate that $r^{(2)}$ exceeds $r^{(1)}$ by 3.0 standard deviations of the total uncertainties, with yet more significant deviations from zero observed for the other two differences of ratios.

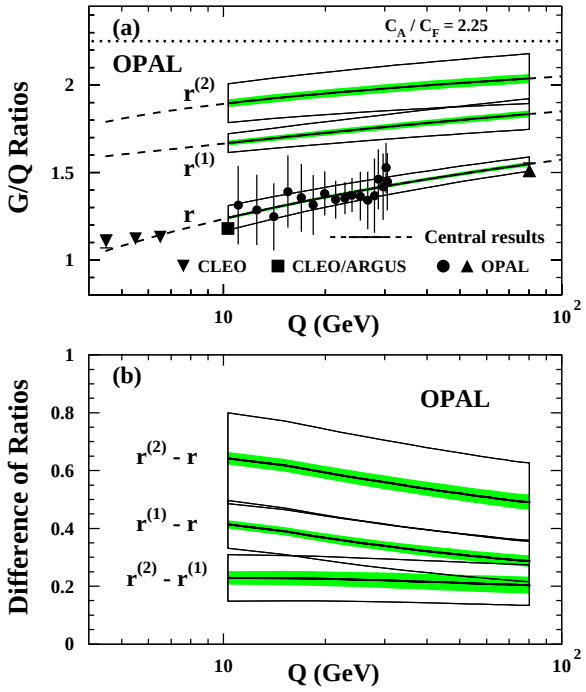

Fig. 9. a The experimental results for r, $r^{(1)}$ and $r^{(2)}$ from Figs. 7 and 8, collected together; **b** the differences between ratios $r^{(2)} - r$, $r^{(1)} - r$ and $r^{(2)} - r^{(1)}$ as a function of scale. The central results are shown by solid curves; the shaded and open bands show the corresponding statistical and total uncertainties, respectively

6.3.2 Comparison to theoretical expressions

The 3NLO analytic predictions of Capella et al. [14] for r, $r^{(1)}$ and $r^{(2)}$ are shown by the long-dashed curves in Figs. 7 and 8. For $Q = 30$ GeV, the ratios are predicted to be 1.73, 1.87 and 2.00, respectively, assuming $n_f = 5$ and $\Lambda = 0.20$ GeV. Thus, the analytic predictions for r and $r^{(1)}$ exceed the corresponding experimental results in (17)–(18) by about 22% and 6%, while the theory agrees with the data, (19), for $r^{(2)}$. Therefore the analytic predictions agree better with the data the higher the level of differentiation of the multiplicity curves. This suggests that higher order corrections are smaller for $r^{(2)}$ than $r^{(1)}$, and for $r^{(1)}$ than r.

We note there are ambiguities in the analytic calculation related to the effective number of active quark flavors and the scale Q at which to evaluate the strong coupling strength. The 3NLO predictions shown here are based on $n_f = 5$ (as stated above) and $Q = E_{c.m.}$. Other plausible choices such as $n_f = 4$ and $Q = E_{c.m.}/4$ change the analytic prediction for r by as much as about 10% and can bring the theoretical curve into better agreement with the data, see Fig. 2 of [9] for example.

A second QCD prediction for r versus scale was recently presented by Lupia and Ochs [13]. This prediction is based on numerical, rather than analytic, techniques, incorporating more accurate phase space limits for the emission of soft gluons and a more complete treatment

of energy conservation than the analytic expression. Unlike the analytic result, a prediction is presented only for r, however, not for $r^{(1)}$ or $r^{(2)}$. We derive a prediction for $r^{(1)}$ from the numerical calculation in the following manner. We begin with numerical predictions for the individual gluon and quark jet multiplicities[7], given in steps of 0.02 units in y with $y = \ln(Q/Q_c)$ where $Q_c = 0.507$ GeV [13]. We make linear interpolations between the points and use the slopes of these lines to estimate $\mathrm{d}N_g/\mathrm{d}y$ and $\mathrm{d}N_q/\mathrm{d}y$, which are then used to determine $r^{(1)}$ as a function of scale Q. We attempted to extend this technique to obtain a prediction for $r^{(2)}$ as well. The derived results for $r^{(2)}$ were very scattered from point to point as a function of Q because of limited numerical precision. We therefore do not quote a prediction for $r^{(2)}$ based on the calculation of [13].

The predictions of the numerical calculation for r and $r^{(1)}$ are shown by the short-dashed-dotted curves in Figs. 7 and 8a. At 30 GeV, the numerical calculation predicts r to be 1.45, in agreement with our measurement at that scale, (17). The corresponding result for $r^{(1)}$ is 1.64, about 7% below the data, (18). For r, the agreement with data is therefore better for the numerical method than for the analytic calculation. The level of agreement of the two predictions with data is similar for $r^{(1)}$. The difference between the analytic and numerical results for r (long-dashed and short-dash-dotted curves in Fig. 7) is believed to arise from the differences in phase space limits and energy conservation noted above. For further discussion, see [12].

Finally, theoretical predictions for r, $r^{(1)}$ and $r^{(2)}$ can be derived from the formalism of Edén and Gustafson [15], using (14). To obtain a prediction for $r^{(1)}$, we begin with the experimental results for the slope of quark jets, $\mathrm{d}N_{q\bar{q}}(L)/\mathrm{d}L$, determined in the manner described in Sect. 6.3.1 for $\mathrm{d}N_{q\bar{q}}(y)/\mathrm{d}y$, with $y = L/2$. We insert this result in (14) to obtain a prediction for $\mathrm{d}N_{gg}(L)/\mathrm{d}L$. Dividing this result by the measured $\mathrm{d}N_{q\bar{q}}(L)/\mathrm{d}L$ yields the prediction for $r^{(1)}$. To obtain a prediction for $r^{(2)}$, we differentiate (14) with respect to L and follow an analogous procedure to that described for $r^{(1)}$. To obtain a prediction for r, we fix the gluon jet multiplicity at 80.2 GeV to the $g_{incl.}$ measurement from OPAL [11]. We then use the prediction for $\mathrm{d}N_{gg}(L)/\mathrm{d}L$ determined as described above to evaluate the gluon jet multiplicity at other scales and divide the result by the 3NLO expression for the quark jet multiplicity fitted to data (solid curve in Fig. 4).

The predictions obtained in this manner are shown by the long-dash-dotted curves in Figs. 7 and 8. The results are seen to be in good overall agreement with the data. We note, however, that these predictions are based on the experimental measurements of quark jet multiplicities. Furthermore, the prediction for r utilizes the measured gluon jet multiplicity at $Q = 80.2$ GeV as stated above. Therefore, the predictions we derive based on [15] are not independent of the data.

[7] We thank Wolfgang Ochs for providing these results

6.4 Measurement of C_A/C_F

Measurements of the energy dependence of unbiased particle multiplicities in gluon and quark jets can also be used to determine an effective value of the ratio of QCD color factors C_A/C_F. Such a possibility was first discussed in [18]. To perform this measurement, we integrate (14) to obtain:

$$\mathrm{N}_{gg}(L) = \mathrm{N}_{gg}(L_0) + \frac{C_A}{C_F}\,\mathcal{F}(L) \quad , \tag{32}$$

with $\mathrm{N}_{gg}(L_0)$ an integration constant which serves as the reference point for $\mathrm{N}_{gg}(L)$, and where

$$\mathcal{F}(L) \equiv \int_{L_0 - c_g + c_q}^{L - c_g + c_q} \left[\left(1 - \frac{\alpha_0 c_r}{x}\right) \frac{\mathrm{d}\,\mathrm{N}_{q\bar{q}}(x)}{\mathrm{d}x}\right] \mathrm{d}x \quad . \tag{33}$$

We evaluate (33) numerically using the experimental results for $\mathrm{d}N_{q\bar{q}}(Q)/\mathrm{d}Q$ discussed in Sect. 6.3.1. As the reference point $\mathrm{N}_{gg}(L_0)$ in (32), we use the direct measurement of gluon jet multiplicity from OPAL [11]. Thus $L_0 = 2\ln(Q_0/\Lambda)$, with $Q_0 = 80.2$ GeV and $\mathrm{N}_{gg}(L_0) = 28.56$ [11]. For Λ we used the fitted result for $\Lambda_{eff.}$ for quark jets from Table 2, $\Lambda = 0.19$ GeV. Note that the results for C_A/C_F are independent of this choice.

A one parameter fit of (32) is made to the gluon jet measurements in Fig. 6a, excluding the CLEO data below 7 GeV, to obtain

$$\frac{C_A}{C_F} = 2.232 \pm 0.008\,(stat.) \pm 0.108\,(syst.) \pm 0.082\,(ref.) \quad , \tag{34}$$

where the first uncertainty is statistical. The second uncertainty is a systematic term evaluated as described in Sect. 7. The third uncertainty is an additional systematic term defined by the difference observed if the CLEO measurement of N_{gg} at 10.3 GeV is used as the reference point, rather than the OPAL measurement at 80.2 GeV. The χ^2 (d.o.f.) of the fit is 29.5 (17). The result of our fit, (34), is consistent with the QCD value $C_A/C_F = 2.25$.

The fitted expression of (32) yields a curve which is almost identical to the 3NLO curve in Fig. 6a: therefore we do not display the fitted curve of (32) in addition. In Fig. 10 we present the result for the event multiplicity in Y events. The data in this figure are the same as in Fig. 3a. The curve is obtained from (4), with $\mathrm{N}_{gg}(k_{\perp,Lu})$ the fitted expression of (32) and $\mathrm{N}_{q\bar{q}}(L, k_{\perp,Lu})$ the measured result from Sect. 6.1. The open band shows the uncertainty of the analytic result, evaluated using the uncertainty from (34) in addition to those shown for the $\mathrm{N}_{q\bar{q}}(L, k_{\perp,Lu})$ terms in Fig. 5. The curve is seen to provide an accurate description of the data to within its uncertainty for θ_1 values larger than approximately 10°. This represents a considerable improvement compared to the results of [42] based on earlier theoretical formalism [17], in which the corresponding fitted analytic expression was found to describe the data for θ_1 values larger than about 60° only (see Fig. 4 of [42]).

To test our technique of determining C_A/C_F, we apply our analysis to parton level Monte Carlo events generated with a c.m. energy of 10 TeV. The parton level

is defined using final-state partons, i.e. those which are present after the termination of the parton shower. We use Herwig version 6.2 with the parameters discussed in Sect. 6.2. Applying our analysis to parton level events with a very large energy tests our method to determine C_A/C_F since the parton level asymptotic result must be consistent with 2.25 for the analysis to be considered valid, see [42] for further discussion. The parton level Herwig events at 10 TeV yield $C_A/C_F = 2.285 \pm 0.010\,(stat.) \pm 0.047\,(ref.)$, where the central value is defined using the Herwig parton level prediction for N_{gg} at 80 GeV as the reference point. The first uncertainty is statistical while the second uncertainty is defined by the difference found if the Herwig prediction for N_{gg} at 10 GeV is used as the reference point instead (i.e. this is analogous to how the third uncertainty of (34) is defined). Thus our one parameter fit method yields an asymptotic result of 2.25 to within the uncertainties associated with the analysis procedure, implying that the similarity of our measurement (34) with the QCD value of C_A/C_F is not merely coincidental. For information, the parton level Herwig result at $E_{c.m.} = 91$ GeV is $2.03 \pm 0.01\,(stat.)$ if the prediction for N_{gg} at 80 GeV is used as the reference point and $2.35 \pm 0.02\,(stat.)$ if the prediction at 10 GeV is used. The analogous results for hadron level Herwig events are 2.34 ± 0.01 and 2.07 ± 0.02, respectively. We therefore observe a much stronger dependence on the choice of the normalization point for the 91 GeV Monte Carlo results than for the 10 TeV results or for the data. The Herwig results at 91 GeV are nonetheless consistent with 2.25, once the systematic uncertainty related to choice of the normalization point is considered.

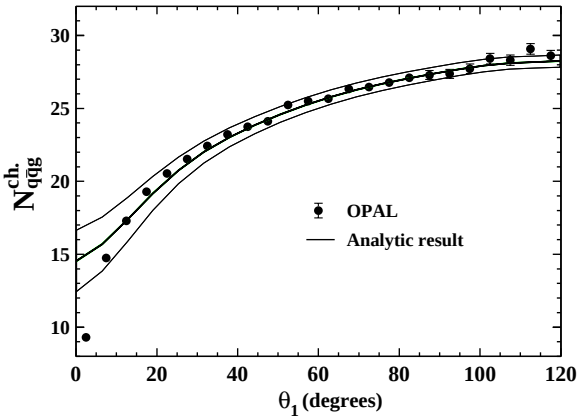

Fig. 10. The mean charged particle multiplicity of three-jet uds flavor Y events from Z^0 decays compared to the analytic expression, (4), for which the gluon jet multiplicity term $N_{gg}(k_{\perp,Lu})$ is determined from a one parameter fit of (32) to unbiased gluon jet data and the quark jet term $N_{q\bar{q}}(L, k_{\perp,Lu})$ is measured. The open band shows the evaluated uncertainty of the analytic result. Note the theory is not expected to be applicable for small values of θ_1 because the events in this case do not have a well defined three jet event structure

7 Systematic uncertainties

To evaluate systematic uncertainties, the analysis was repeated with the following changes to the standard analysis. The full differences between the standard results and those found using each of these changes were used to define symmetric systematic uncertainties. For items 1, 5 and 7, listed below, the largest of the described differences with respect to the standard result was assigned as the systematic uncertainty. The uncertainties were added in quadrature to define the total systematic uncertainties.

For the measurement of the gluon jet multiplicity $N^{ch.}_{gg}$ (Fig. 6), the following changes were made. Items 1-3 and 5 in this list were also applied to the study of two-jet events, see Sect. 6.1. The items are listed in roughly decreasing order of the size of their contribution to the total uncertainties of the $N^{ch.}_{gg}$ measurements.

1. The jet finding was performed using the Cambridge and Luclus jet finders, rather than the Durham jet finder. For the Luclus jet finder, we did not perform a direct measurement of the biased quark jet terms $N^{ch.}_{q\bar{q}}(J, k_{\perp,Lu})$ since it is not obvious how to relate the resolution scale d_{join} to $p_{\perp,Lu}$ as mentioned in Sect. 6.1. Instead we used the analytic expression, (13), for the determination of the gluon jet multiplicities $N^{ch.}_{gg}(L)$. The difference between the Durham and Cambridge results was used to define the systematic uncertainty due to jet finding for the two jet event measurements shown in Fig. 5.
2. Tracks selected for the uds tagging procedure were required to have a signed impact parameter which satisfied $d_{sign}/\sigma_{d_{sign}} > 1.5$, rather than $d_{sign}/\sigma_{d_{sign}} > 3.0$; at the same time we required $|\cos(\theta_{\rm thrust})|$ to be less than 0.8, rather than 0.9. The purpose of these two changes was to increase the purity of tagged uds events; the estimated uds event purity increased to 85.1% from 78.5% while the number of selected events decreased to 8610 from 22 365. The more restrictive condition on $|\cos(\theta_{\rm thrust})|$ yields a higher uds purity because a larger fraction of tracks in an event traverses the silicon microvertex detector.
3. The Herwig Monte Carlo event generator was used to determine the corrections for initial-state photon radiation, detector response, and uds event and gluon jet misidentification, rather than Jetset. For this purpose, we used version 5.9 of the program [38] with the parameter values in [32], except that the cluster mass cutoff CLMAX was increased from 3.40 to 3.75 GeV/c^2 to improve the model's description of the mean charged particle multiplicity in inclusive hadronic Z^0 decays.
4. For our measurements of the gluon jet multiplicities $N^{ch.}_{gg}$ based on (15), we used the analytic expression, (13), rather than the direct measurement of $N^{ch.}_{q\bar{q}}(L, k_{\perp,Lu})$.
5. Charged tracks alone were used for the data and Monte Carlo samples with detector simulation, rather than charged tracks plus electromagnetic clusters. As an additional check on the track selection, the standard analysis (tracks and clusters) was varied by increasing the minimum transverse momentum of charged tracks

with respect to the beam axis from from 0.05 GeV/c to 0.15 GeV/c.

For the two-jet events (Fig. 5), the dominant systematic term was from item 1 at low $p_{\perp,Lu}$ and from item 3 at intermediate and high $p_{\perp,Lu}$.

In addition to the above, the following changes were made to evaluate systematic uncertainties for the ratios r, $r^{(1)}$ and $r^{(2)}$.

6. The ARGUS and 91 GeV LEP measurements of $N^{ch.}_{e^+e^-}$ were excluded from the fit of quark jet multiplicity (solid curve in Fig. 4). These two data points have the smallest uncertainties of the results in the fit and were excluded to potentially maximize a systematic variation. The results of the alternate fit are $\Lambda_{eff.} = 0.261 \pm 0.061$, $K = 0.154 \pm 0.014$ and χ^2 (d.o.f.) = 1.5 (14). Besides the evaluation of a systematic uncertainty for r, $r^{(1)}$ and $r^{(2)}$, this alternate result for $N^{ch.}_{q\overline{q}}(L)$ was used to derive the MLLA prediction shown by the dashed curve in Fig. 5.
7. Y events with $50^\circ \leq \theta_1 \leq 120^\circ$ were used in the fit of gluon jet multiplicity versus scale, rather than $35^\circ \leq \theta_1 \leq 120^\circ$; as an alternate check, the ratios were determined after increasing the inclusive gluon jet measurement from CLEO at 10.3 GeV by its one standard deviation total uncertainty, then decreasing it by one standard deviation, and repeating the same operation for the inclusive gluon jet measurement from OPAL at 80.2 GeV.

For the ratios, the largest systematic terms were from items 1, 6 and 7. The contributions of items 2 and 5 were by comparison negligible, with the other items intermediate. For our measurement of C_A/C_F (Sect. 6.4), increasing and decreasing the inclusive OPAL measurement at 80.2 GeV by one standard deviation (item 7) provided the largest contribution to the overall uncertainty. Item 1 provided the second largest contribution while the contributions of the other items were much smaller.

For the data listed in Tables 4 and 5 and the corresponding results in Figs. 6, 7 and 9a, the systematic uncertainty evaluated for each bin was averaged with the results from its two neighbors to reduce the effect of bin-to-bin fluctuations. The single neighbor was used for bins on the endpoints of the distributions.

8 Summary

We have presented measurements of the mean charged particle multiplicity of three-jet "Y events" as a function of the opening angle between the two lowest energy jets, θ_1, and of two-jet events as a function of the resolution scale separating the two- and three-jet event classes. The measurements were performed using the Durham jet finder. The Cambridge and Luclus jet finders were used as systematic checks for the three-jet measurements and the Cambridge jet finder for the two-jet measurements. The two- and three-jet events were selected from a sample of Z^0 decays to light flavor (u, d or s) quark-antiquark pairs produced in e^+e^- annihilations. The restriction to light quark flavors improves the correspondence of the data to theoretical predictions.

We use these data to test recent theoretical formalism [15,16] for particle multiplicity in jets which accounts for biases introduced by the jet finding criteria. We find that the theoretical prediction for particle multiplicity in biased two-jet events, (13), agrees fairly well with our two-jet event data. In conjunction with the results from Y events, the two-jet data are used to extract the multiplicity of *unbiased* gluon jets at a variety of scales. Of two possible forms proposed in [16] to obtain this information – one [15] based on the definition of gluon jet transverse momentum from the Lund group and the other [17] from the Leningrad group – we find clear preference for the former because of the consistency of the derived results with direct measurements of unbiased gluon jet multiplicity from the CLEO [7,8] and OPAL [9]- [11] Collaborations as well as with Monte Carlo expectations.

The unbiased gluon jet multiplicities extracted with this technique, which range in scale from 11.1 to 30.5 GeV, are compared to corresponding results from light unbiased quark jets. In conjunction with direct measurements of unbiased gluon jet multiplicity at 10.3 and 80.2 GeV from CLEO and OPAL, we determine the ratio of charged particle multiplicities between gluon and quark jets, $r = N_g/N_q$, and the corresponding ratios of slopes and of curvatures, $r^{(1)} = (dN_g/dy)/(dN_q/dy)$ and $r^{(2)} = (d^2N_g/dy^2)/(d^2N_q/dy^2)$, as a function of energy scale $y = \ln(Q/\Lambda)$, with Q the jet energy and Λ the QCD scale parameter, set to 0.20 GeV in our study. At 30 GeV, a typical scale in our analysis, we find $r = 1.422 \pm 0.006 \pm 0.051$, $r^{(1)} = 1.761 \pm 0.013 \pm 0.070$ and $r^{(2)} = 1.98 \pm 0.02 \pm 0.13$, and at 80 GeV $r = 1.548 \pm 0.008 \pm 0.041$, $r^{(1)} = 1.834 \pm 0.016 \pm 0.088$ and $r^{(2)} = 2.04 \pm 0.02 \pm 0.14$, where the first uncertainty is statistical and the second systematic. These results are based on QCD analytic parametrizations [14,36] of the scale dependence of particle multiplicity in jets. We also present results which utilize polynomial parametrizations, or which assume no functional dependence for the growth of gluon jet multiplicity with scale, and obtain consistent results albeit with larger uncertainties. Our results are in agreement with the QCD prediction that $r^{(2)}$ should be closer to its asymptotic value of 2.25 than $r^{(1)}$, and $r^{(1)}$ closer to 2.25 than r, for the finite energies of our experiment. Our result for $r^{(2)}$ is the first experimental determination of that quantity.

The results for r, $r^{(1)}$ and $r^{(2)}$ are compared to recent QCD predictions based on analytic [14] and numerical [13] techniques, as well as to predictions derived from the formalism of [15]. We find overall agreement between the experimental and theoretical results.

Finally, we use the results on the energy dependence of N_g and N_q to determine an effective value of the ratio of QCD color factors, C_A/C_F. We find $C_A/C_F = 2.23 \pm 0.14$ (total), consistent with the QCD value of 2.25.

Acknowledgements. We thank Igor Dremin, Patrick Edén and Valery Khoze for helpful comments. We particularly wish to

thank the SL Division for the efficient operation of the LEP accelerator at all energies and for their close cooperation with our experimental group. We thank our colleagues from CEA, DAPNIA/SPP, CE-Saclay for their efforts over the years on the time-of-flight and trigger systems which we continue to use. In addition to the support staff at our own institutions we are pleased to acknowledge the Department of Energy, USA, National Science Foundation, USA, Particle Physics and Astronomy Research Council, UK, Natural Sciences and Engineering Research Council, Canada, Israel Science Foundation, administered by the Israel Academy of Science and Humanities, Minerva Gesellschaft, Benoziyo Center for High Energy Physics, Japanese Ministry of Education, Science and Culture (the Monbusho) and a grant under the Monbusho International Science Research Program, Japanese Society for the Promotion of Science (JSPS), German Israeli Bi-national Science Foundation (Fig), Bundesministerium für Bildung und Forschung, Germany, National Research Council of Canada, Research Corporation, USA, Hungarian Foundation for Scientific Research, OTKA T-029328, T023793 and OTKA F-023259, Fund for Scientific Research, Flanders, F.W.O.-Vlaanderen, Belgium.

References

1. HRS Collaboration, M. Derrick et al., Phys. Lett. B **165**, 449 (1985)
2. OPAL Collaboration., G. Alexander et al., Phys. Lett. B **265**, 462 (1991)
3. ALEPH Collaboration, D. Buskulic et al., Phys. Lett. B **384**, 353 (1996)
4. DELPHI Collaboration, P. Abreu et al, Z. Phys. C **70**, 179 (1996)
5. S. Catani et al., Phys. Lett. B **269**, 432 (1991)
6. T. Sjöstrand, Comp. Phys. Comm. **28**, 229 (1983)
7. CLEO Collaboration, M.S. Alam et al., Phys. Rev. D **46**, 4822 (1992)
8. CLEO Collaboration, M.S. Alam et al., Phys. Rev. D **56**, 17 (1997)
9. OPAL Collaboration, G. Alexander et al., Phys. Lett. B **388**, 659 (1996)
10. OPAL Collaboration, K. Ackerstaff et al., Eur. Phys. J. C **1**, 479 (1998)
11. OPAL Collaboration, G. Abbiendi et al., Eur. Phys. J. C **11**, 217 (1999)
12. I.M. Dremin, J.W. Gary, Phys. Rep. **349**, 301 (2001)
13. S. Lupia, W. Ochs, Phys. Lett. B **418**, 214 (1998)
14. A. Capella et al., Phys. Rev. D **61**, 074009 (2000)
15. P. Edén, G. Gustafson, JHEP **9809**, 015 (1998)
16. P. Edén, G. Gustafson, V.A. Khoze, Eur. Phys. J. C **11**, 345 (1999)
17. Yu.L. Dokshitzer, V.A. Khoze, S.I. Troyan, Sov. J. Nucl. Phys. **47**, 881 (1988)
18. DELPHI Collaboration, P. Abreu et al, Phys. Lett. B **449**, 383 (1999)
19. OPAL Collaboration, G. Abbiendi et al., Eur. Phys. J. C **17**, 373 (2000)
20. See, for example, Yu.L. Dokshitzer et al., Basics of Perturbative QCD, ed. J. Tran Thanh Van, Editions Frontiéres, Gif-sur-Yvette, 1991; V.A. Khoze, W. Ochs, Int. J. Mod. Phys. A **12**, 2949 (1997)
21. Yu.L. Dokshitzer et al., JHEP **9708**, 001 (1997)
22. JADE Collaboration, W. Bartel et al., Z. Phys. C **33**, 23 (1986)
23. UA1 Collaboration, G. Arnison et al., Phys. Lett. B **123**, 115 (1983); CDF Collaboration, F. Abe et al., Phys. Rev. D **45**, 1448 (1992); OPAL Collaboration, R. Akers et al., Z. Phys. C **63**, 197 (1994)
24. OPAL Collaboration, K. Ahmet et al., Nucl. Instr. and Meth. A **305**, 275 (1991)
25. P.P. Allport et al., Nucl. Instr. and Meth. A **346**, 476 (1994)
26. OPAL Collaboration, G. Alexander et al., Z. Phys. C **52**, 175 (1991)
27. S. Brandt et al., Phys. Lett. **12**, 57 (1964); E. Fahri, Phys. Rev. Lett. **39**, 1587 (1977)
28. OPAL Collaboration, M.Z. Akrawy et al., Phys. Lett. B **261**, 334 (1991)
29. OPAL Collaboration, G. Alexander et al., Phys. Lett. B **265**, 462 (1991)
30. T. Sjöstrand, Comp. Phys. Comm. **82**, 74 (1994)
31. J. Allison et al., Nucl. Instr. and Meth. A **317**, 47 (1992)
32. OPAL Collaboration, G. Alexander et al., Z. Phys. C **69**, 543 (1996)
33. OPAL Collaboration, M.Z. Akrawy et al., Z. Phys. C **47**, 505 (1990)
34. S. Bentvelsen, I. Meyer, Eur. Phys. J. C **4**, 623 (1998)
35. ALEPH Collaboration, D. Buskulic et al., Phys. Lett. B **384**, 353 (1996); SLD Collaboration, K. Abe et al., Phys. Lett. B **386**, 475 (1996); DELPHI Collaboration, P. Abreu et al., Phys. Lett. B **479**, 118 (2000); OPAL Collaboration, G. Abbiendi et al., Eur. Phys. J. C **16**, 185 (2000)
36. I.M. Dremin, J.W. Gary, Phys. Lett. B **459**, 341 (1999)
37. J.W. Gary, Phys. Rev. D **49**, 4503 (1994)
38. G. Marchesini et al., Comp. Phys. Comm. **67**, 465 (1992)
39. G. Corcella et al., JHEP **0101**, 010 (2001)
40. OPAL Collaboration, R. Akers et al., Z. Phys. C **68**, 179 (1995)
41. ARGUS Collaboration, H. Albrecht et al., Z. Phys. C **54**, 13 (1992)
42. J.W. Gary, Phys. Rev. D **61**, 114007 (2000)